The Pennsylvania State University

The Graduate School

Department of Aerospace Engineering

Effect of Wing Tip Configuration on the Strength and Position of a Rolled-Up Vortex

NASA ~~Grant~~ NGR 39-009-111

A thesis in

Aerospace Engineering

by

Raghuveera Padakannaya

Submitted in partial fulfillment
of the requirements
for the degree of

Master of Science

March 1970

Approved:

Head of the Department of Aerospace
Engineering, Thesis Advisor

Professor of Aerospace Engineering

ACKNOWLEDGMENTS

The author wishes to express his gratitude to Dr. Barnes W. McCormick, Jr., Chairman of the Department of Aerospace Engineering for his invaluable suggestions and guidance of this work. Thanks are also due to R. Husted, for his help during the experiments. Gratitude is also expressed to the Engineering Department workshop staff for their help in the building of model wings.

The work reported in this thesis was sponsored by the National Aeronautics and Space Administration (Langley) Contract No. NGR 39-009-111.

TABLE OF CONTENTS

LIST OF TABLES

LIST OF FIGURES

Figure Page

NOMENCLATURE

a	= Core radius [radius where $v(r)$ is a maximum]
A	= Aspect ratio = b^2/s
b	= Wing span of rectangular wing of aspect ratio 4.5
c	= Local wing chord
C_ℓ	= Section lift coefficient
L	= Lift per unit span
n	= exponent in vorticity distribution, equation 13
r	= Radial coordinate
R	= radius
s	= Semispan
S	= Wing area
t	= Time
u	= Velocity component in direction of "r"
v	= Velocity component normal to "u"
V	= Free stream velocity
w	= Half radius = r at which $\zeta = \zeta_o/2$
W	= Downwash velocity
x,y,z	= Coordinates of the control point
y'	= Spanwise coordinate of the wing

$$\left.\begin{array}{l} X = x/y_v \\ Y = y/y_v \\ Z = z/y_v \end{array}\right\}$$ Nondimensional coordinates of the control point

Z_1 = Distance downstream of wing trailing edge

y_v = Semiwidth of the horseshoe vortex

θ = Droop angle

α = Angle of attack

$\gamma(2/n)$ = Gamma function of argument $(2/n)$

Γ = $\Gamma(\eta)$ strength of circulation at the section η,

= Circulation at any radius r

Γ_o = Mid-span value of bound circulation (strength of vortex)

Γ_∞ = Total circulation (as $r \rightarrow \infty$)

η = $y'/(b/2)$ Nondimensional spanwise coordinate

ν = Kinematic viscosity

ρ = Density

ζ = Vorticity at any radius r

ζ_o = Center value of ζ ($r = 0$)

Subscripts

i,j = Number of chordwise and spanwise locations of control points

ℓ,m = Number of chordwise and spanwise locations of vortices

ABSTRACT

This thesis studies the effects of different wing tip configurations on its rolled-up vortex. The spanwise load distribution on plain rectangular wings and on wings with drooped tips was calculated by vortex lattice theory, to determine the effects of the droop on the strength and the location of the vortex. The load distribution on wings with drooped tips shows that the stronger vortex moves from the tip of the wing to the hinge of the drooped tip as the droop angle increases. The experimental program was to determine how the vortex sheet shed initially from the wing's trailing edge rolls up and how these trailing vortices dissipate downstream of the wings. The results were obtained for wings with 0°, 70°, 80°, 90°, 110° droop angles, at approximately the same lift coefficient. The experimental results confirmed the movement of the stronger vortex from the tip of the wing to the hinge of the drooped tip as the droop angle increases.

The experimental results are presented as contours of constant vorticity to show the rolling-up of the trailing vortex sheet behind the different models. Results are also presented to show the strength and the induced velocity profiles of the rolled-up vortex generated by the models.

CHAPTER I

INTRODUCTION

1.1 General Introduction

Any airfoil or lifting surface produces a system of trailing vortices as a result of the lift or circulation variation along the span. This trailing sheet of free vortices, which represents a surface of discontinuity, is unstable and tends to roll-up rapidly behind the lifting surface to form a pair of discrete vortex filaments. Thus the trailing wake some distance behind a rotor blade will consist of a root and a tip vortex, in opposite sense to each other. The tip vortex is concentrated while the root vortex is diffuse. A rotor blade can intersect the tip vortex generated by a preceding blade under certain flight conditions. The rotor blade-vortex interaction is one of the three mechanisms postulated in the literature as the cause of blade slap, the term used for the sharp, cracking sound associated with helicopter rotors. Expanded use of helicopters for both civilian and military operations and the importance that the noise can play in the success or failure of these operations, makes it important to avoid blade vortex interaction.

1.2 Statement of the Problem

The object of this study was to develop a tip configuration which will displace the rolled-up vortex vertically from the tip plane a sufficient distance so that a following blade will not intersect the vortex. Since it is not practical to survey the geometry of the trailing vortex of a rotating blade, fixed wing models having different tip shapes were studied. This study is both analytical and experimental in nature. The analytical part determines the spanwise load distribution on the drooped tip wing models by lifting surface theory with the objective of determining qualitatively the strength and spanwise location of the rolled-up vortex behind wings. The experimental program was to determine how the vortex sheet shed initially from the trailing edge of the drooped tip wings rolls-up and how these trailing vortices dissipate downstream of the wings. The experimental investigation utilized a small vorticity meter to measure the vorticity distribibition in the rolling-up vortex sheet to determine the size and the strength of the vortex.

CHAPTER II

PREVIOUS INVESTIGATIONS

Under certain flight conditions, a helicopter rotor blade intersects the trailing vortex system shed by other blades. Recently, model studies (Reference 6) of a two bladed helicopter rotor flow patterns in a water tunnel have shown that, in the low forward speed ranges, portions of the tip vortex shed at the front of the disc lie above the following rotor blade in such a manner that the following blade(s) can intersect one or more of the vortices. Vapor trail studies, Reference 5, have also shown that the trailing vortex and the following blade can interact. This rotor blade/vortex interaction is one of the mechanisms postulated for "Blade Slap," the term used for the sharp cracking sound associated with helicopter rotors.

At low forward speeds the blade slap is due to the rapid changes in angle of attack and subsequent lift change produced by blade/vortex interaction. At high forward speeds blade slap or bang may be due to rapid changes in drag produced on the advancing blade as a result of the local supersonic flow which can occur near the tip of the advancing blade. In Reference 11, an attempt was made to eliminate blade bang or slap. The objective of this study was to modify the induced velocity distribution of the trailing vortex without appreciable effect on the strength of the bound circulation on the blade. Vorticity measurements behind ten blade tip configurations were made in a wind-tunnel, using a vortex meter described in Reference 14. This vortex meter is capable of surveying the entire wake of a vortex system. It consists of a small spinner with four unpitched vanes that cause the spinner to rotate when placed in a rotational flow field. The strength of the vorticity at any point is obtained by measuring rotational speed of the spinner. The results of Reference 11 demonstrated that the velocity induced within a trailing vortex system could be substantially reduced at the price of some increased drag by the use of a porous tip, which should lead to the elimination of blade banging. One particular tip, a 60° sweep delta shape, effectively diffused the tip vortex with no performance penalty.

The tip section of a helicopter rotor blade plays a much more important role in providing lift than the wing tip area of an airplane, because the dynamic pressure is much higher near the blade tip than on inboard portions of the blade. Therefore, improvements in blade tip aerodynamic characteristics can result in appreciable improvements in helicopter performance. Conventional blades are designed to generate as much lift as possible and in practice the section lift increases right up to within a few percent of the blade radius. Beyond that point it falls off rapidly so that a very large change of bound circulation occurs causing intense shedding of vorticity. By changing the blade geometry near the tip this lift decay can be made more gradual, spreading the vorticity shed over a greater length of blade. Some limited success in this direction was achieved (Reference 5) on an S-61 helicopter rotor on which the standard blade tips were replaced for the outer 6% radius with tapered planform tips designed to reduce the spanwise loading gradient. There was a substantial reduction in noise level in addition to a performance gain.

In Reference 8, a number of blades designed to have an improved blade loading at the tips, were tested and indicated that the best acoustic and aerodynamic performances were obtained with a twisted trapezoidal tip designed to provide elliptic aerodynamic loading at the tip. It was expected that elliptical loading would reduce the induced velocity of the tip vortex.

In Reference 15, noise measurements made on a UH-1D helicopter rotor with thinner, cambered profiles near the tip used for delaying the compressibility effects, indicated a significant reduction in noise level. Noise measurements made in the NASA-Ames 40 ft x 80 ft wind-tunnel with the same rotors confirmed this. It was also found that the noise of the thin tip rotor apparently increases less rapidly with increasing Mach Number than that of the standard rotor and hence greater reduction where indicated at higher Mach Numbers.

CHAPTER III

ANALYTICAL STUDY

The purpose of this part of the study is to determine the spanwise load distribution on drooped tip wing models, in an effort to determine, qualitatively, the effect of the droop on the strength and location of the rolled-up vortex.

Various methods of analyzing the finite wing exists. These methods range from Prandtl's simplified lifting line theory to the various lifting surface theories such as those of Weissinger and Falkner. The mathematical model of the finite wing consists of a chordwise distribution of vorticity representing the lifting surface and a trailing wake consisting of a vortex sheet. Prandtl's lifting line theory is applicable to wings of vanishingly small chord which permits the contraction of the chordwise vorticity distribution into a single bound vortex of varying strength along the span. The model for the calculation of downwash induced at the wing by the trailing vortex system, consists of a single bound vortex of varying strength in the spanwise direction from which is shed the continuous trailing vortex sheet. The downwash is calculated along the bound vortex line and then the lift at any section can be calculated by the application of one Kutta-Joukowski theorem.

In the Weissinger approximation, the bound circulation is concentrated along the one-quarter-chord line and the boundary condition of the resultant velocity being tangential to the wing surface is satisfied along the three-quarter-chord line of the wing. This simple method gives surprisingly accurate results.

Any lifting surface theory involves finding a potential flow to satisfy the Kutta condition along the trailing edge and at the same time satisfying the boundary condition that the normal velocity components vanish everywhere on the wing surface. As there is an abrupt change in the direction of the trailing edge at the droop as shown in Figure 1, lifting surface methods were felt to be more reliable in predicting the load distribution.

Falkner's vortex lattice method is used as this arrangement permits greater flexibility in the range of planforms that can be treated. In Reference 1, Falkner assumed a general mathematical formula for continuous loading on a wing which is equivalent to a double Fourier series with unknown coefficients. In order to evaluate the unknown coefficients the continuous loading was split up into a regular pattern of horseshoe vortices, the strengths which are proportional to unknown coefficients. The boundary condition of zero normal velocity was satisfied at a few pivotal points chosen which resulted in a set of simultaneous equations for the unknown coefficients.

The general assumptions made in the present analysis are:

(1) The fluid through which the wing moves is assumed to be inviscid and incompressible.

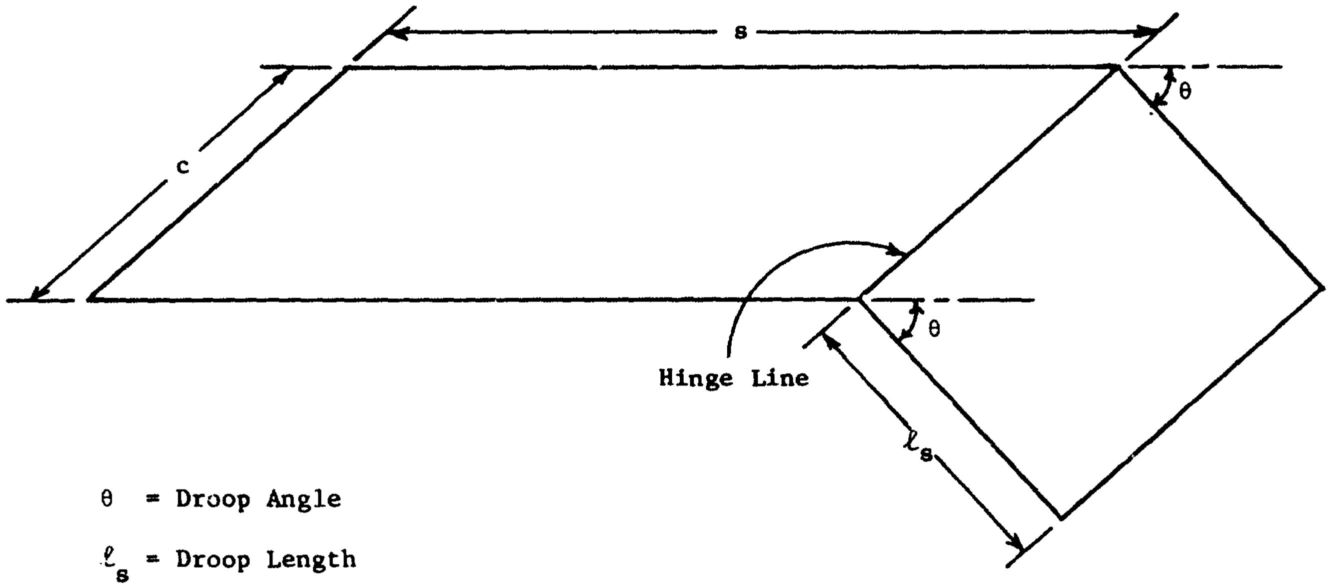

FIGURE 1 DROOPED TIP WING MODEL

(2) The wing is assumed to be of negligible thickness.

(3) The trailing vortex is assumed to be straight and parallel to the direction of flight.

Actually a trailing vortex sheet induces a velocity approximately normally to itself over its entire surface, and hence it does not trail parallel to the direction of flight but is deflected downward. Because the induced velocities increase with distance behind the wing the deflection of the sheet increases towards an asymptotic value as we move downstream. The assumption of an undeflected trailing vortex sheet is valid for wings at ordinary lift coefficient.

The continuous distribution of circulation is approximated by a number of horseshoe vortices, each extending over a small fraction of the span and placed so as to form a rectangular lattice. Figure 2 shows a typical example. In the vortex lattice theory both the spanwise and the chordwise loadings are made stepwise discontinuous. The boundary condition which fixes the spanwise variation of circulation is that the slope induced in the flow field by the downwash normal to the plate due to the horseshoe vortices shall be equal to the slope of the plate with respect to the free stream at specified points (control points). The Kutta condition is satisfied by choosing some control points downstream of all of the bound vortices.

Referring to Figure 3, the complete downwash, $W_{\ell m}$, at a point P(X,Y,Z) due to a rectangular vortex of strength $\Gamma_{\ell m}$ is

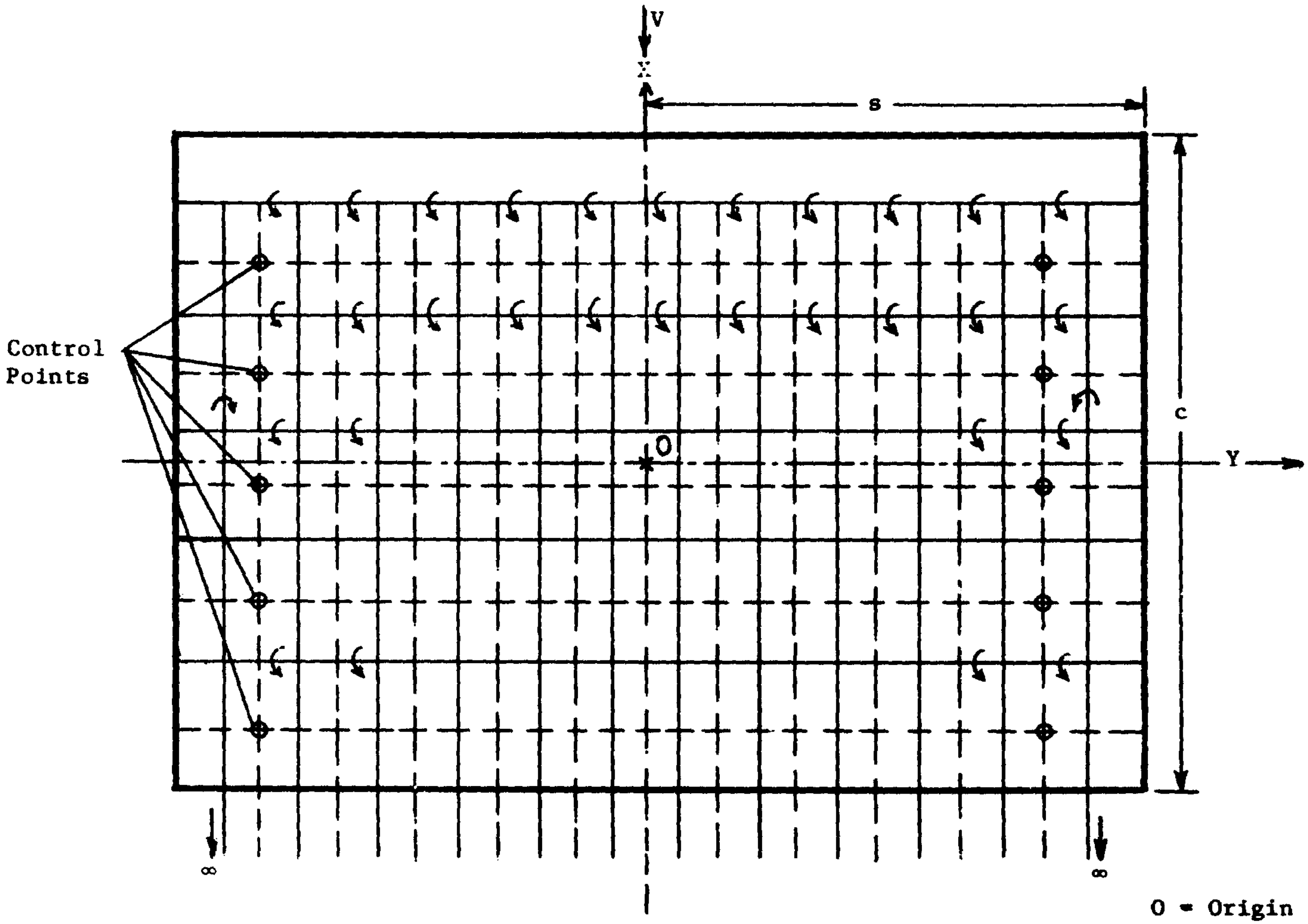

FIGURE 2 TYPICAL VORTEX PATTERN AND LOCATION OF CONTROL POINTS

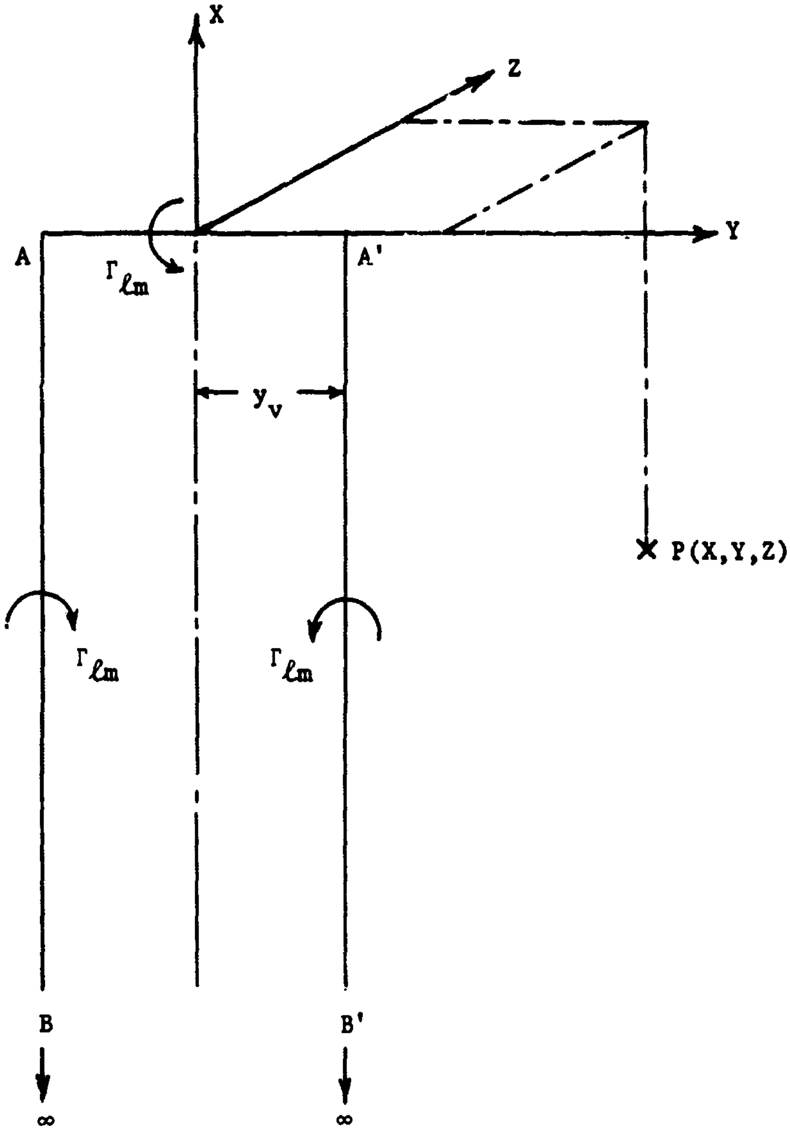

$X = x/y_v$

$Y = y/y_v$

$Z = z/y_v$

y_v = Semiwidth of the vortex

FIGURE 3 GEOMETRIC RELATIONSHIP DEFINING THE INDUCED VELOCITY BY A RECTANGULAR VORTEX ELEMENT

$$W_{\ell m} = \frac{\Gamma_{\ell m}}{4\pi y_v}\left[-\frac{X}{(X^2+Z^2)}\left\{\frac{(Y+1)}{\sqrt{X^2+(Y+1)^2+Z^2}}-\frac{(Y-1)}{\sqrt{X^2+(Y-1)^2+Z^2}}\right\}\right.$$

$$-\frac{(Y-1)}{(Y-1)^2+Z^2}\left\{1-\frac{X}{\sqrt{X^2+(Y-1)^2+Z^2}}\right\}$$

$$\left.+\frac{(Y+1)}{(Y+1)^2+Z^2}\left\{1-\frac{X}{\sqrt{X^2+(Y+1)^2+Z^2}}\right\}\right]$$

$$= \frac{\Gamma_{\ell m}}{2y_v}\left[\frac{H(\ell,m)}{2\pi}\right] \tag{1}$$

where X,Y,Z are the (nondimensional) coordinates of the point P.

y_v = semiwidth of the horseshoe vortex.

When the point P lies in the plane of the wing (Z = 0) the expression for the downwash reduces to the following simple form.

$$W_{\ell m} = \frac{\Gamma_{\ell m}}{4\pi y_v}\left[\frac{(Y+1)\sqrt{X^2+(Y-1)^2}-2X-(Y-1)\sqrt{X^2+(Y+1)^2}}{Y(Y-1)(Y+1)}\right] \tag{2}$$

The total downwash W at a chosen control point is obtained by summing the downwashes due to individual vortices. The boundary condition at the control point can be written as follows:

$$\frac{W}{V} = \frac{1}{V}\sum_{\ell,m} W_{\ell m} = \tan\alpha \simeq \alpha \text{ (for small } \alpha)$$

$$= \frac{1}{2Vy_v}\sum_{\ell,m}\Gamma_{\ell m}\left(\frac{H(\ell,m)}{2\pi}\right) \tag{3}$$

where ℓ and m are the number of vortices in the chordwise and spanwise directions respectively. The summation is taken over all the horseshoe vortices.

The number of control points chosen is equal to the number of unknown horseshoe vortices. The control points are chosen midway between two successive vortices as the downwash tends to infinity in the neighborhood of each vortex. As stated previously, the Kutta condition of smooth, tangential flow at the trailing edge is satisfied by the satisfaction of the boundary condition at the control point near the trailing edge.

The satisfaction of the boundary condition at each control point results in an equation for the unknown vortex strengths. By satisfying the boundary condition at all the control points a system of linear equations for the unknown vortex strengths is obtained.

This system of equations can be written as

$$\frac{1}{2Vy_v} \sum_{\ell,m} \Gamma_{\ell m} \frac{H_{ij}(\ell,m)}{2\pi} = \alpha_{ij} \tag{4}$$

where $\alpha_{ij} = \alpha$ = angle of attack of the wing. Where i and j are the number of control points in the chordwise and the spanwise directions respectively.

$$\frac{1}{2\pi(2Vy_v)} [\Gamma_{11}H_{11}(1,1) + \Gamma_{12}H_{11}(1,2) + \ldots + \Gamma_{1m}H_{11}(1,m) + \Gamma_{21}H_{11}(2,1)$$

$$+ \ldots + \Gamma_{2m}H_{11}(2,m) + \ldots + \Gamma_{\ell m}H_{11}(\ell,m)] = \alpha_{11}$$

$$\frac{1}{2\pi(2Vy_v)}\,[\Gamma_{11}H_{12}(1,1) + \Gamma_{12}H_{12}(1,2) + \ldots + \Gamma_{1m}H_{12}(1,m) + \Gamma_{21}H_{12}(2,1)$$

$$+ \ldots + \Gamma_{2m}H_{12}(2,m) + \ldots + \Gamma_{\ell m}H_{12}(\ell,m)] = \alpha_{12}$$

$$\vdots$$

$$\frac{1}{2\pi(2Vy_v)}\,[\Gamma_{11}H_{ij}(1,1) + \Gamma_{12}H_{ij}(1,2) + \ldots + \Gamma_{1m}H_{ij}(1,m) + \Gamma_{21}H_{ij}(2,1)$$

$$+ \ldots + \Gamma_{2m}H_{ij}(2,m) + \ldots + \Gamma_{\ell m}H_{ij}(\ell,m)] = \alpha_{ij} .$$

For the wings with drooped tips, control points and vortices were also placed on the droop. The boundary condition for the control points on the droop then becomes

$$W/V = \alpha \cos \theta \tag{5}$$

W = downwash normal to the droop

θ = angle of the droop

α = angle of attack of the plain wing

V = free stream velocity.

Hence on the droop

$$\alpha_{ij} = \alpha \cos \theta .$$

The above system of simultaneous equations can be solved to obtain the unknown vortex strengths.

Knowing the circulation of each section of the wing, the section lift coefficient can be determined by the application of the Kutta-Joukowski theorem at each section.

$$L = \text{lift per unit span} = \rho V \Gamma$$

$$= \frac{1}{2} \rho V^2 c C_\ell \qquad (6)$$

$$\therefore C_\ell = \text{sectional lift coefficient} = 2\Gamma/Vc \qquad (7)$$

where V = free stream velocity

c = local chord

ρ = density

$\Gamma = \Gamma(\eta)$ = strength of circulation at the section considered

$= \sum_\ell \Gamma_{\ell m}$, m corresponding to the section considered.

The IBM 360/67 high speed digital computer at The Pennsylvania State University Computation Center was used to obtain the numerical solution to the problem.

The set of simultaneous equations (4) was solved by the Gauss-elimination method to obtain the strengths of the vortics. The coefficients of these simultaneous equations, and hence the strengths of vortices, depend on the number of vortices and their locations in the chordwise and spanwise directions. The vortex locations and control point locations are handled as input data. The control points are located midway between successive vortices. This method permits an arbitrary number of vortices and their locations and at the same time maintain the correct number and locations of control points as the control points are located midway between successive vortices. The optimum number of vortices and their locations were selected on the basis of the required accuracy in comparison with earlier results, for a plain rectangular wing. The present method of calculation requires about 20 secs of computer time for a rectangular wing replaced by 100 vortices (without using symmetry property of load distribution) and about 45 secs of computer time for the drooped tip wings replaced by about 130 unknown vortices.

CHAPTER IV

EXPERIMENTAL INVESTIGATION

The investigation of the formation of a trailing vortex system behind finite wing models involved wind-tunnel studies. Since it is not practical to survey the geometry of the trailing vortex of a rotating blade, fixed wing models with different droop angles were designed. Figure 1 shows the droop angle.

Because of wind tunnel size restrictions, the wing semispan of the plain rectangular wing model was limited to about 18 inches. The model blade chord dimension was 8 inches. For the drooped tip models the length of droop was about 7.5 inches.

The wind-tunnel studies were conducted in The Pennsylvania State University's subsonic wind tunnel. The tunnel has a rectangular test section 3 feet by 3 feet with a maximum tunnel speed of about 300 mph. The wing models were mounted vertically on a six-component strain gage balance used to obtain the lift of the wing models.

Model testing included models having droop angles of 0°, 70°, 80°, 90° and 110°. A vortex probe, developed by May, was used to measure the vorticity in four successive transverse planes behind the wings. These planes were located 1 1/2, 5, 15 and 20 inches behind the trailing edge. Each transverse plane was surveyed with the wings at the same lift. The vortex probe used is shown in Figure 4. It consists of four unpitched steel vanes mounted on an aluminum spinner. The spinner is press fitted into a steel shaft that is free to rotate in a set of jewel bearings. A hole drilled through the shaft, perpendicular to its axis of rotation, is filled with plexiglass to reduce windage losses. A photovoltaic cell and a miniature light bulb are placed in line with the hole and are separated by the shaft. As the shaft rotates, two pulses of light pass through the hole each revolution. These pulses are sensed by the photovoltaic cell and counted electronically as cycles per second. Since there are two counts per revolution, the spinner RPM is obtained by multiplying the cycles per second by 30.

The vortex probe is subject to error due to friction and windage losses along with error caused by the spinner's finite size. From the vane calibration curve for the vortex meter using a spinner with 3/8 inch diameter vanes, the efficiency is 0.78, for the wind tunnel data collected in this thesis at a tunnel speed of 65 mph.

With the use of the probe positioning mechanism shown in Figure 5, any plane perpendicular to the flow in the wind-tunnel could be surveyed. The position of the vortex probe could be varied both in the horizontal (Y-direction) and vertical (Z-direction). Its location in rectangular coordinates was given by means of two mechanical counters, one for the up and down movement and the other for the right and left movement. Each counter was driven by a synchro that was wired to a transmitting unit. The two transmitting

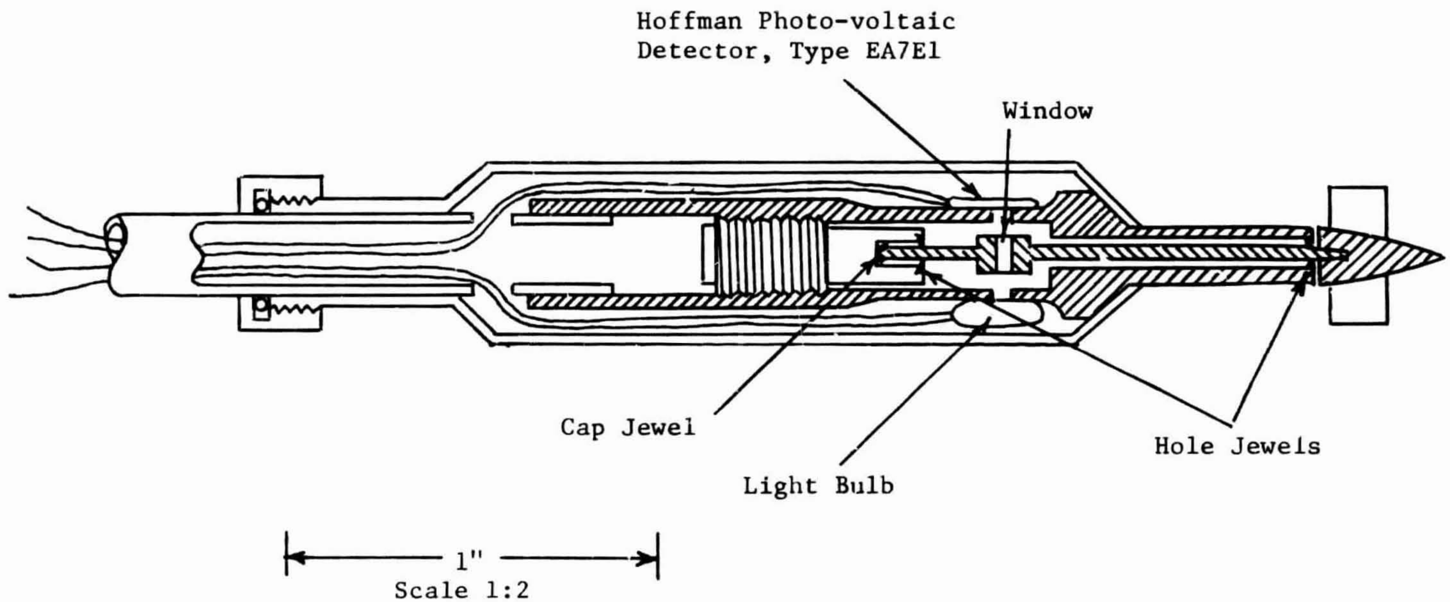

FIGURE 4 VORTEX PROBE

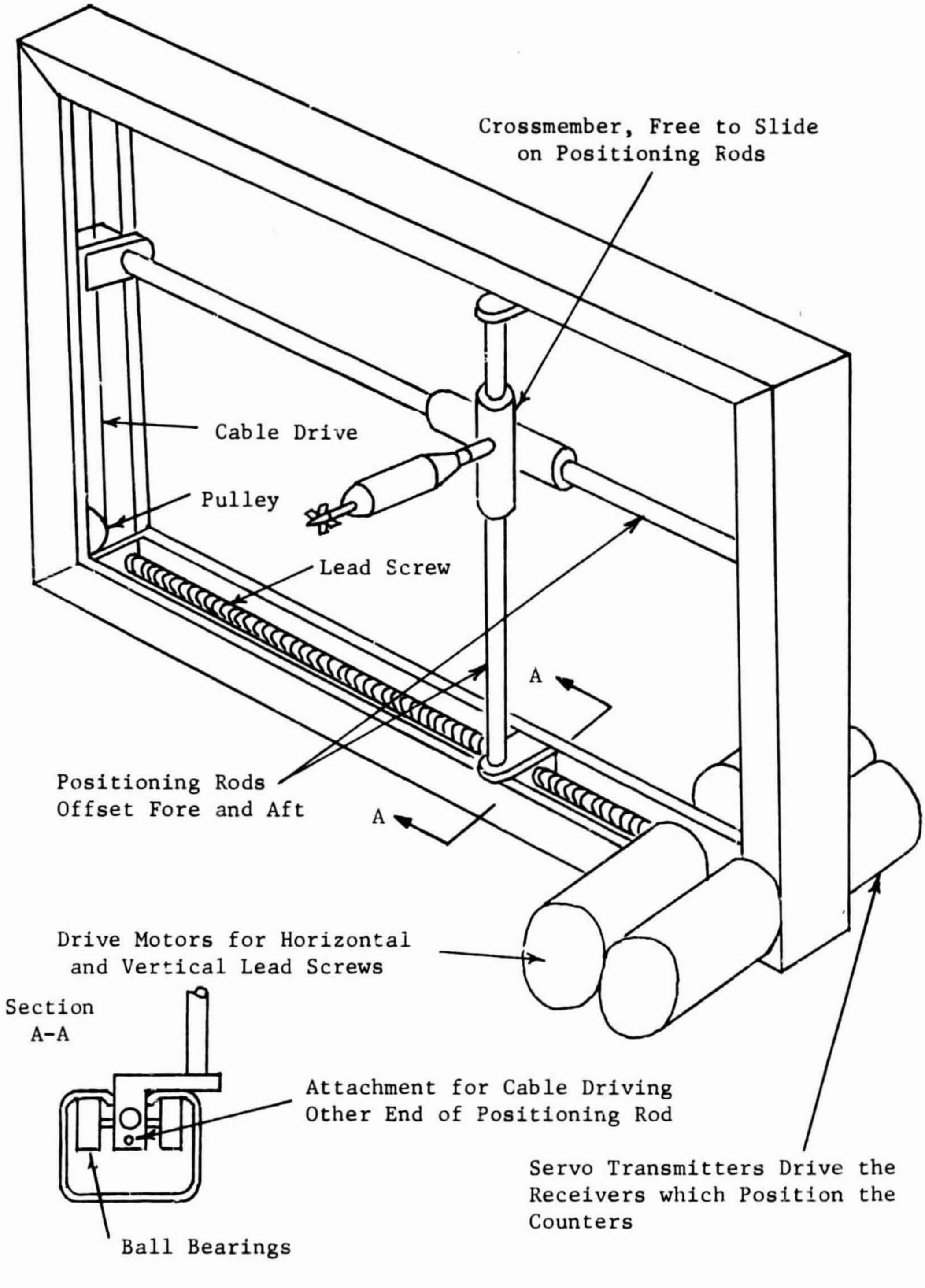

FIGURE 5 PROBE POSITIONING MECHANISM

units were connected to separate lead screws that positioned the probe in both the vertical and horizontal direction. One inch diaplacement of the vortex probe in either coordinate direction corresponds to 400 counts on the mechanical counter.

Before each plane was surveyed, the calibration of the vortex probe was checked to make sure that the probe was operating satisfactorily. With the probe clear of the wing, a calibrating device which consisted of a fixed set of pitched vanes was mounted ahead of the probe to impart rotation to the flow. Tunnel speed was increased slowly and the output from the vanes was noted. When the probe was calibrated, the set of pitched vanes caused it to register a count of about 400 cps at a tunnel speed of 75 mph. Calibrations were performed periodically as a check on the friction losses in the probe bearings. To eliminate any error caused by improper lubrication, the probe was oiled after every hour of testing. The vorticity measurements for the different wing models were at the same lift.

After the calibration check of the vorticity meter, the wing was positioned to the desired angle of attack and tunnel was brought up to 65 mph. For measurement downstream of the wing, where the vorticity had rolled-up, it was sometimes difficult to locate the vortex. This was accomplished by tracing the path of the vortex with a tuft on the end of a rod from the trailing edge aft to the survey plane. The center of the rolled-up portion of the vortex sheet is located by traversing the wake both vertically and horizontally until the spinner reached its maximum rotational speed which was displayed on the electronic counter. With the Y-coordinate fixed at the value corresponding to the center of the vortex, the vorticity distribution was then surveyed in the Z-direction (along the wing span).

This survey was then used to determine what planes perpendicular to the trailing edge of the wing contained vorticity distribution useful for plotting contours of constant rotational speed. Data points were taken at increments varying from 1/16 inch to 1/8 inch depending on the counter readings, the smaller increment being in the region of higher readings.

It has been found from earlier experiments that the roll-up of the trailing vortex sheet is complete at a downstream distance of about two chords. Hence to determine the strength and the induced velocity of the rolled-up vortex, vorticity measurements were made at the plane 20 inches (2 1/2 chords) downstream of the trailing edge of the wing. For this measurement, the vortex probe was first positioned sideways and vertically until a nearly maximum count was displayed on the counter. Then holding Z constant a run was made by varying Y in small increments, about 1/16 inch. The counts per second read from the electronic counter was then plotted against the Y reading, giving a symmetrical curve about the Y-value. This Y-value was then set, and another run made in the Z-direction would thus pass through the center of the vortex. In the case of drooped tip wings two rolled-up vortices exist, one at the tip of the wing and the other at the hinge line of the droop.

CHAPTER V

DISCUSSION OF RESULTS

5.1 Analytical Results

The spanwise load distribution, on the wings considered, was determined for an angle of attack of 0.1 Radian. Since the strength of the circulation obtained by the vortex lattice method depends on the location and the number of vortices along the span and the chord of the wings, calculations were done with different locations of vortices and control points in the case of plain rectangular wings. The results of these calculations are shown in Figure 6. As shown in this figure, merely increasing the number of vortices does not improve the accuracy of the results. This figure shows the importance of the chordwise locations of the vortices. Table 1 indicates the spanwise and chordwise locations of the vortices for these calculations. It was found that 19 vortices of 0.1s width each, along the span and 5 vortices along the chord, placed at 0.05c, 0.25c, 0.45c, 0.65c, 0.85c are sufficient to give accurate results, in comparison with earlier results (Reference 13) in the case of plain rectangular wing. For the subsequent calculations, combination (5) of Table 1 was used. Lift curve slopes of rectangular wings of different aspect ratios were determined from the spanwise load distribution calculated at an angle of attack of 0.1 Radian. Figure 7

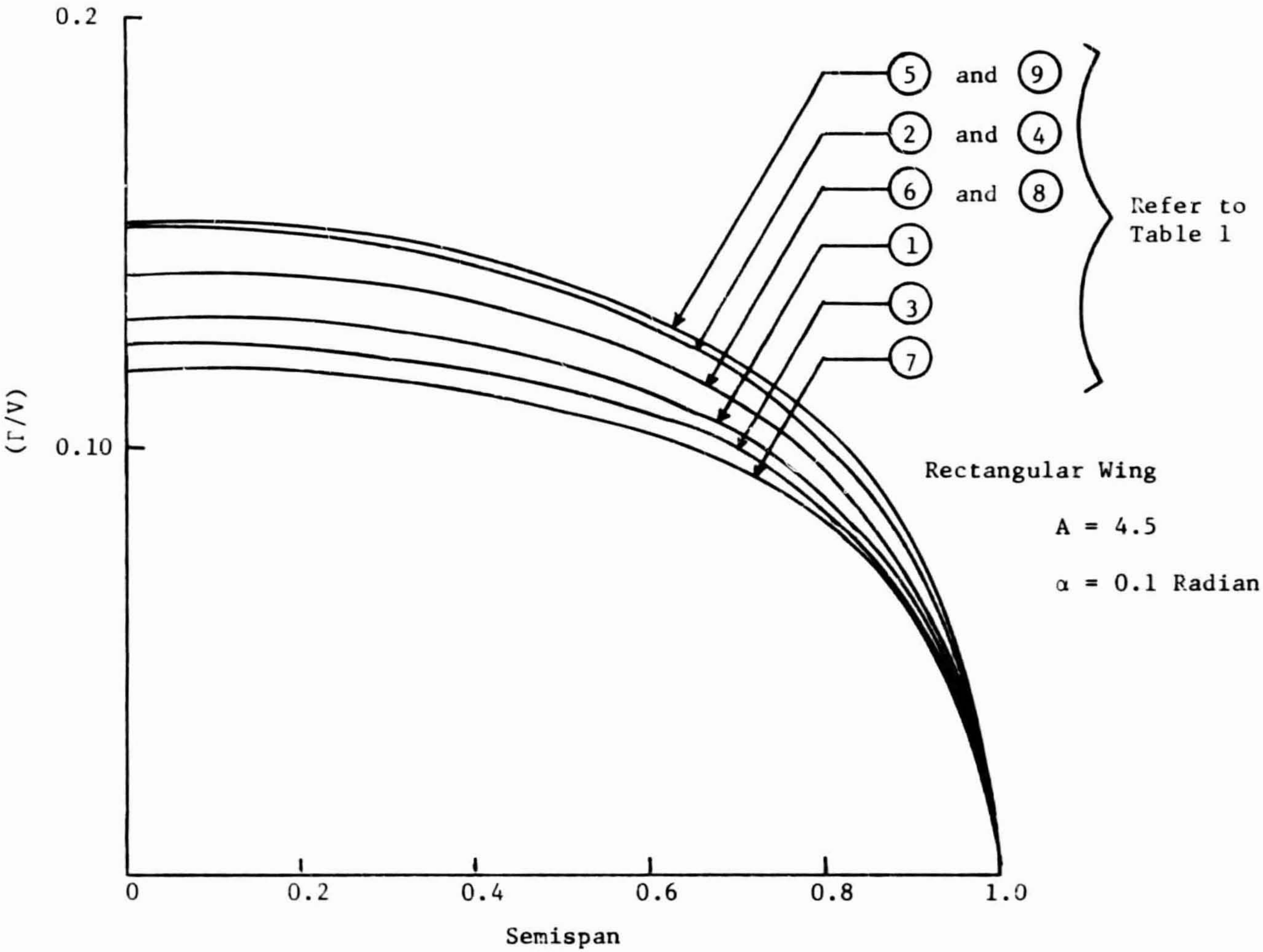

FIGURE 6 EFFECT OF THE NUMBER AND VARIATION OF VORTICES

TABLE 1

EFFECT OF THE NUMBER AND LOCATION OF VORTICES ON RECTANGULAR WING OF A = 4.5

Total Number of Vortices		Spanwise Location of Vortices $\eta = y'/(b/2)$ on the Semispan	Chordwise Location of Vortices (XV/c)	C_L at 0.1 Radian
(1)	76	0.0, 0.1, 0.2, 0.3, 0.4, 0.5, 0.6, 0.7, 0.8, 0.9	0.1, 0.3, 0.5, 0.7	0.318
(2)	76	0.0, 0.1, 0.2, 0.3, 0.4, 0.5, 0.6, 0.7, 0.8, 0.9	0.05, 0.3, 0.55, 0.8	0.365
(3)	95	0.0, 0.1, 0.2, 0.3, 0.4, 0.5, 0.6, 0.7, 0.8, 0.9	0.05, 0.2, 0.35, 0.5, 0.65	0.305
(4)	95	0.0, 0.1, 0.2, 0.3, 0.4, 0.5, 0.6, 0.7, 0.8, 0.9	0.05, 0.25, 0.45, 0.65, 0.85	0.365
(5)	105	0.0, 0.1, 0.2, 0.3, 0.4, 0.5, 0.6, 0.7, 0.8, 0.9, 0.96	0.05, 0.25, 0.45, 0.65, 0.85	0.375
(6)	114	0.0, 0.1, 0.2, 0.3, 0.4, 0.5, 0.6, 0.7, 0.8, 0.9	0.05, 0.2, 0.35, 0.5, 0.65, 0.8	0.343
(7)	133	0.0, 0.1, 0.2, 0.3, 0.4, 0.5, 0.6, 0.7, 0.8, 0.9	0.1, 0.2, 0.3, 0.4, 0.5, 0.6, 0.7	0.271
(8)	171	0.0, 0.1, 0.2, 0.3, 0.4, 0.5, 0.6, 0.7, 0.8, 0.9	0.1, 0.2, 0.3, 0.4, 0.5, 0.6, 0.7, 0.8, 0.9	0.343
(9)	195	0.0, 0.05, 0.1, 0.15, 0.2, 0.25, 0.3, 0.35, 0.4, 0.45, 0.5, 0.55, 0.6, 0.65, 0.7, 0.75, 0.8, 0.85, 0.9, 0.95	0.05, 0.25, 0.45, 0.65, 0.85	0.372

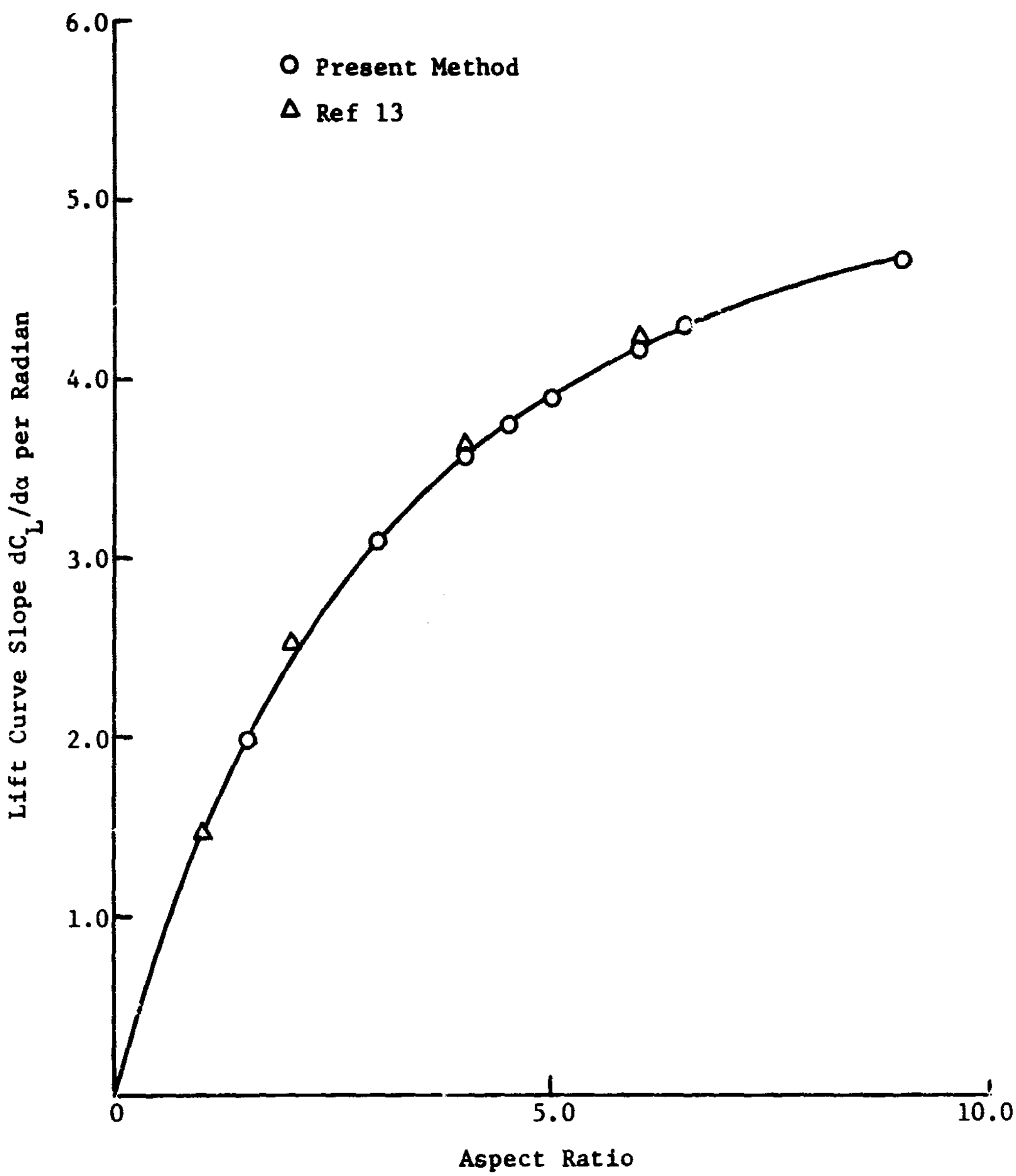

FIGURE 7 VARIATION OF LIFT CURVE SLOPE WITH ASPECT RATIO FOR RECTANGULAR WINGS

shows the variation of lift curve slope with aspect ratio for flat rectangular wings. Included in this figure are the results of Reference 13. The results of Reference 13 were obtained by replacing the wings by 84 vortices and satisfying the boundary condition at only six control points. It can be seen that the results compare favorably. This figure also shows that for plain rectangular wings, the results do not depend very much on the number of control points where the boundary condition is satisfied. Figure 8 shows the spanwise variation of the lift coefficient of flat rectangular wings for different aspect ratios.

The computer program written for the plain rectangular wings was extended to determine the spanwise load distribution on wings with drooped tips. Figure 9 shows the spanwise variation of circulation for the drooped tip wings. The variation of circulation along the wing span must be accompanied by the shedding of vorticity from the wing. These trailing vortices which are shed from the wing are a consequence of Helmholtz's theorem of vortex continuity. The strength of the trailing vortex shed is proportional to the $(d\Gamma/ds)$, the slope of the curve of circulation vs. span. Figure 10 shows the variation of $(d\Gamma/ds)$ near the tip and the hinge line of the drooped tip wings. It is clear from this figure that for θ, the droop angle, up to approximately 45° and less, the slope of the predicted spanwise load distribution is higher near the tip of the wing than at the hinge line. This shows that a stronger vortex is located near the tip and a weaker secondary vortex is located at the hinge line. As the droop angle increases beyond 45°, the loading becomes

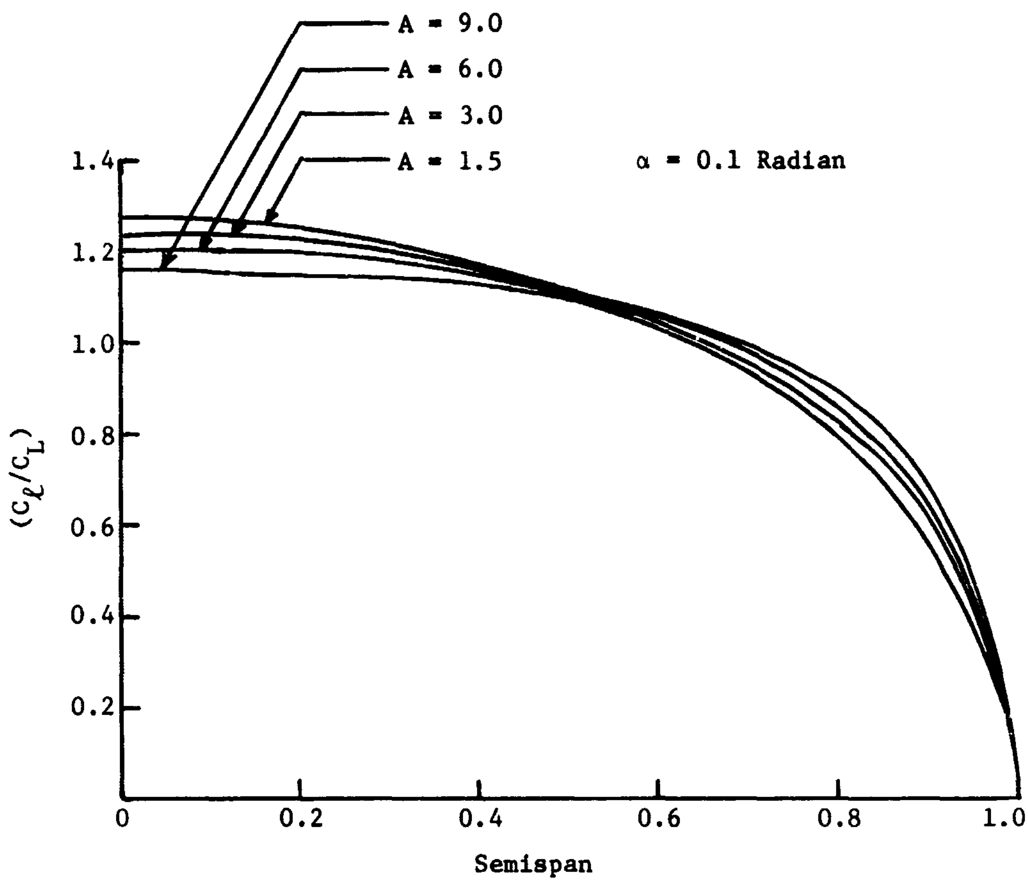

FIGURE 8 EFFECT OF ASPECT RATIO ON LOADING OF FLAT RECTANGULAR WINGS

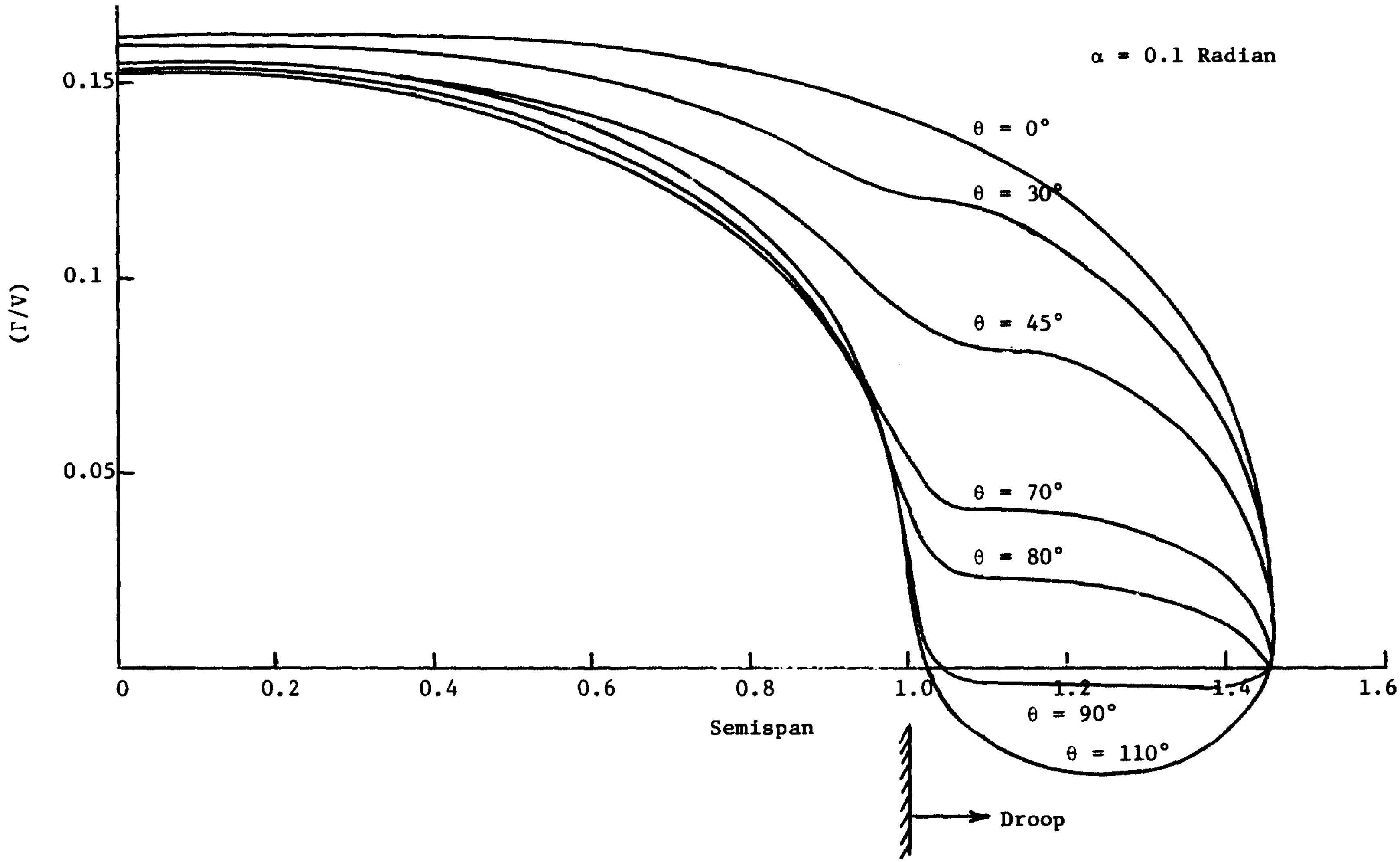

FIGURE 9 LOAD DISTRIBUTION ON WINGS WITH DROOPED TIPS

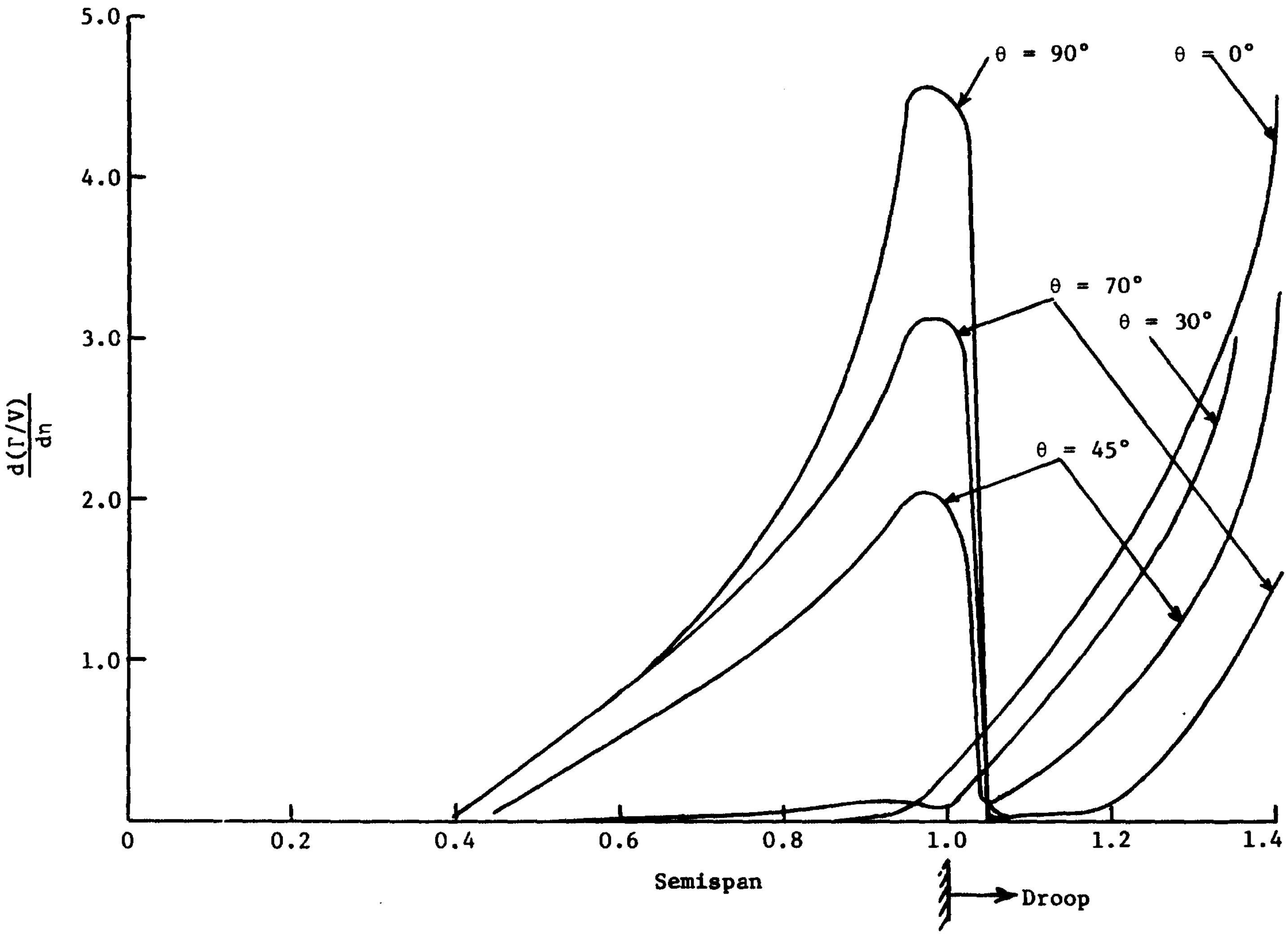

FIGURE 10 SLOPE OF LOAD DISTRIBUTION ALONG THE SPAN OF DROOPED TIP WINGS

weaker near the tip and the stronger vortex moves towards the hinge line from the tip. The spanwise load distribution also shows that the lift of the wing reduces as the droop angle increases, at the same angle of attack.

5.2 Force Measurements

The lift of the wing models were obtained using a six component strain gage balance. The results plotted as C_L vs. α are shown in Figure 11. As seen in this figure, the lift, at the same angle of attack, reduces as the droop angle increases.

Table 2 gives the theoretical and experimental values of the lift coefficient for the wing models. The theoretical values were calculated with the assumption that the normal force on the droop was a linear function of the angle of incidence of the droop for the flat wings. The theoretical values of the lift coefficient for the drooped tip wings are somewhat low in comparison with the experimental values.

5.3 Vortex Measurements

All the vorticity data presented are uncorrected for probe calibration or finite probe size. Reference 11 indicated that at the test speed of 65 mph the vortex meter reads approximately 0.78 of the true rotational velocity of the fluid. Lift values were held approximately constant for different wing configurations. Vortex measurements were made at four stations behind the wing models to

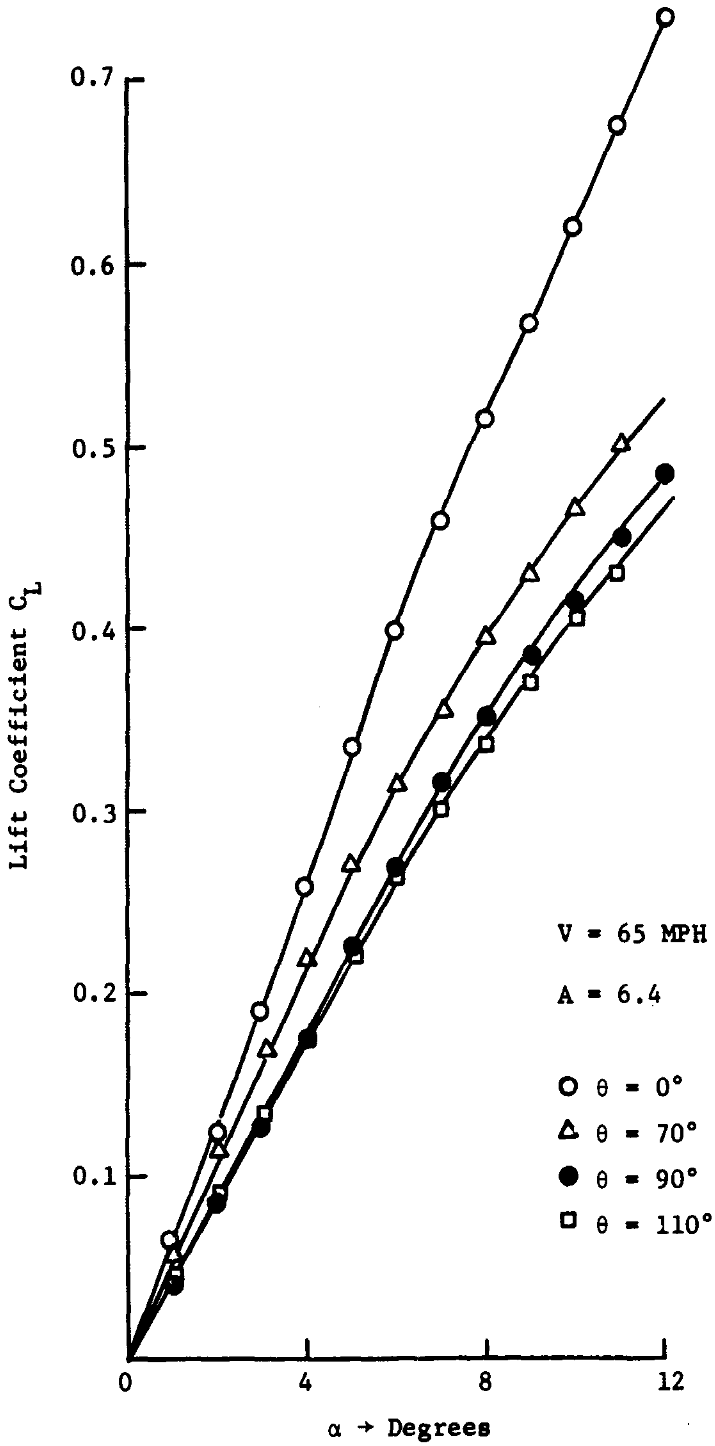

FIGURE 11 C_L VS. α FOR THE WING MODELS

TABLE 2

EFFECT OF DROOPED TIP ON LIFT CURVE SLOPE, $dC_L/d\alpha$ (per Radian)

	Aspect Ratio 6.4		
θ	$\left(\frac{dC_L}{d\alpha}\right)_{EXPTL}$	$\left(\frac{dC_L}{d\alpha}\right)_{TH}$	$\left(\frac{dC_L}{d\alpha}\right)_{TH,\ CORRECTED}$
0°	3.8	4.27	3.98
70°	3.0	2.8	2.54
80°	2.65	2.82	2.57
90°	2.58	2.67	2.43
110°	2.55	2.70	2.46

$$\left(\frac{dC_L}{d\alpha}\right)_{TH,\ CORRECTED} = \left(\frac{dC_L}{d\alpha}\right)_{TH} \times \left(\frac{5.7}{2\pi}\right)$$

determine how the trailing vortex sheet rolls up and diffuses downstream. The results are plotted as contours of constant vorticity and are shown in Figures 12, 13, 14, 15, 16.

In the case of all the drooped tip wings except the one with a droop angle of 110° two vortices, one at the hinge line of the droop and the other at the tip of the droop, are present. Even at a distance of about 20% of the chord behind the trailing edge well defined vortices exist at the tip and the hinge line of the droop. At a distance of about 75% chord behind the wings completely rolled-up vortices exist both at the tip and the hinge line of the droop. In the case of drooped tip wings the tip vortex moves up and towards the hinge line as the vortex moves downstream. As can be seen from these figures the strength of the tip vortex decreases with increase in droop angle from 0° to 110° and there is no noticeable tip vortex in the case of the wing with a droop angle of 110°. The strength of the vortex at the hinge line of droop increases with the increase in droop angle from 70° to 110°.

The vorticity measurements made at a distance of 20 inches downstream (about 2 1/2 chords) were to obtain the vorticity distribution, ζ, at the center section of the completely rolled-up vortex of the model wings. Figure 17 shows the vorticity in the rolled-up tip vortex for the model wings. Figure 18 shows the vorticity in the rolled-up vortex located at the hinge line of the drooped tip wings. It was observed experimentally that the stronger rolled-up vortex is located at the tip of the droop for the droop angle of 70°, though the predicted spanwise load distribution

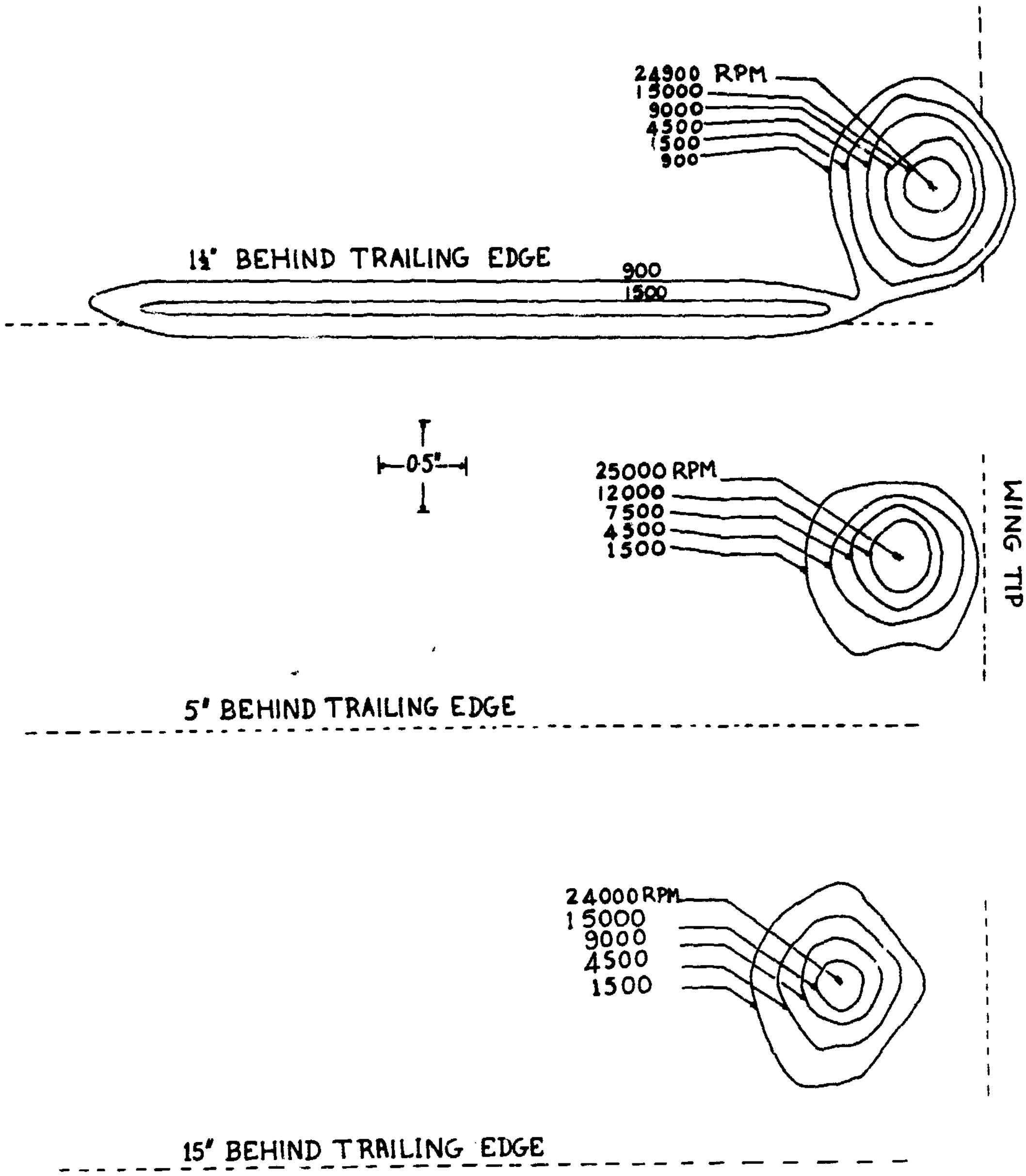

FIGURE 12 VORTICITY CONTOURS FOR PLAIN RECTANGULAR WING, $\theta = 0°$

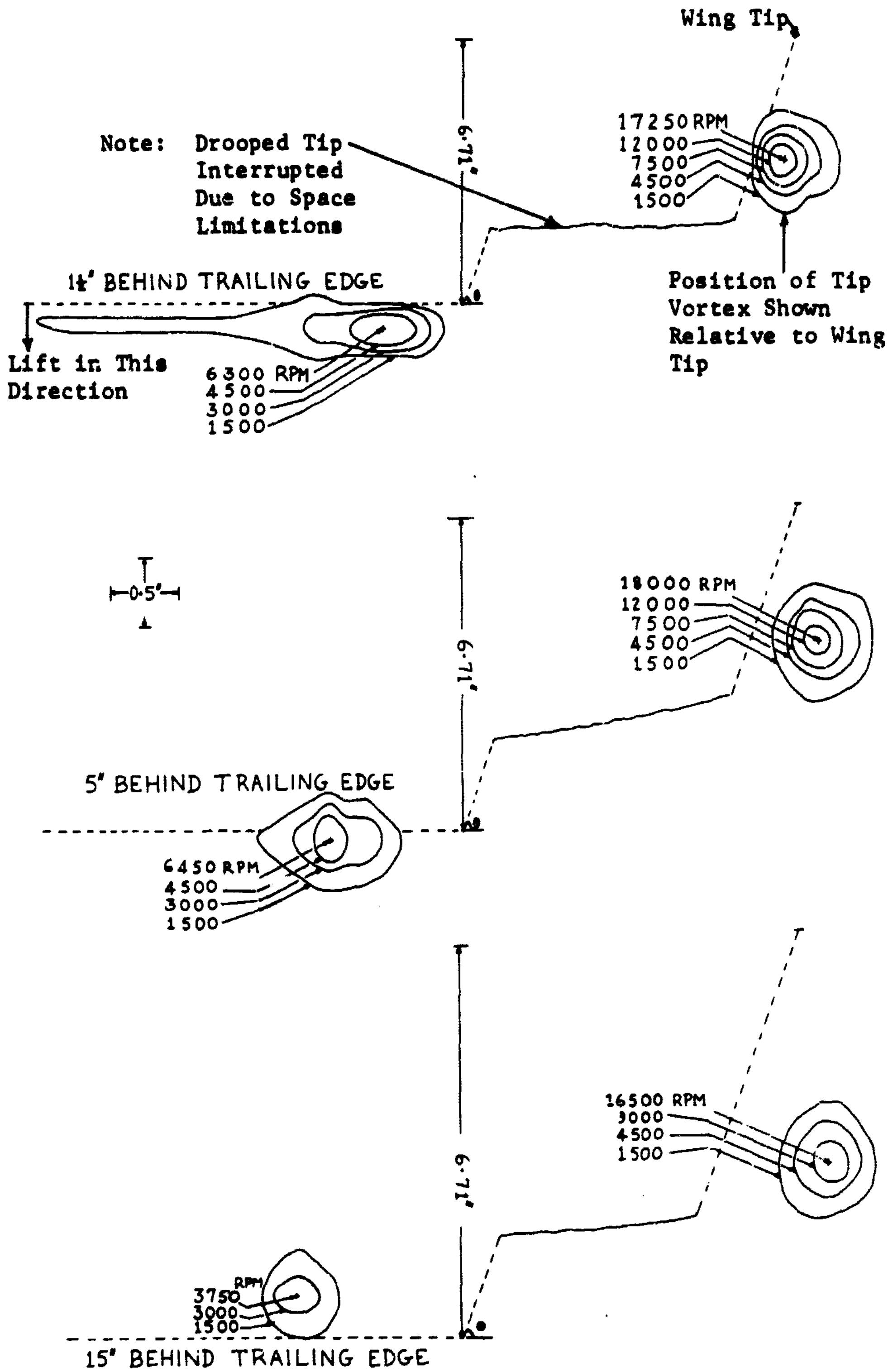

FIGURE 13 VORTICITY CONTOURS FOR DROOPED TIP WING, θ = 70°

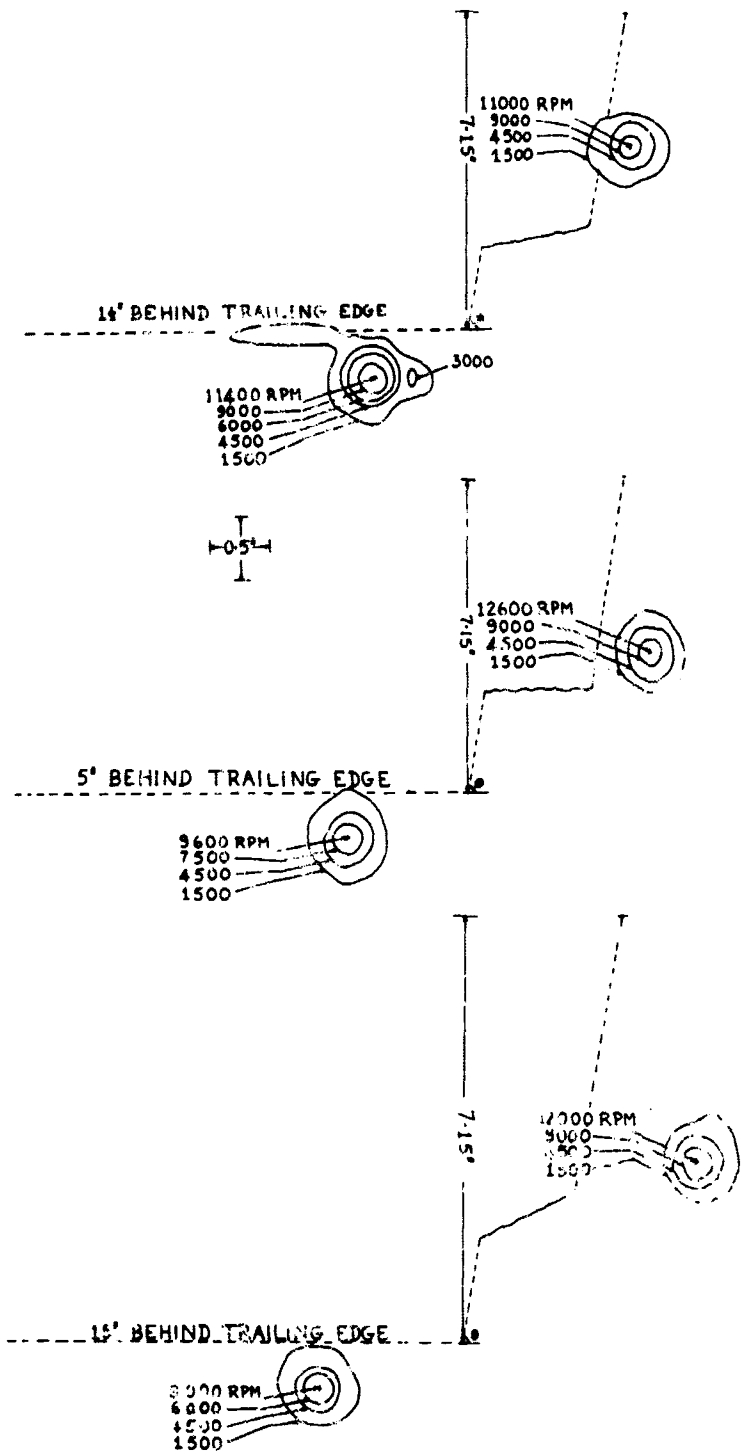

FIGURE 14 VORTICITY CONTOURS FOR DROOPED TIP WING, θ = [illegible]°

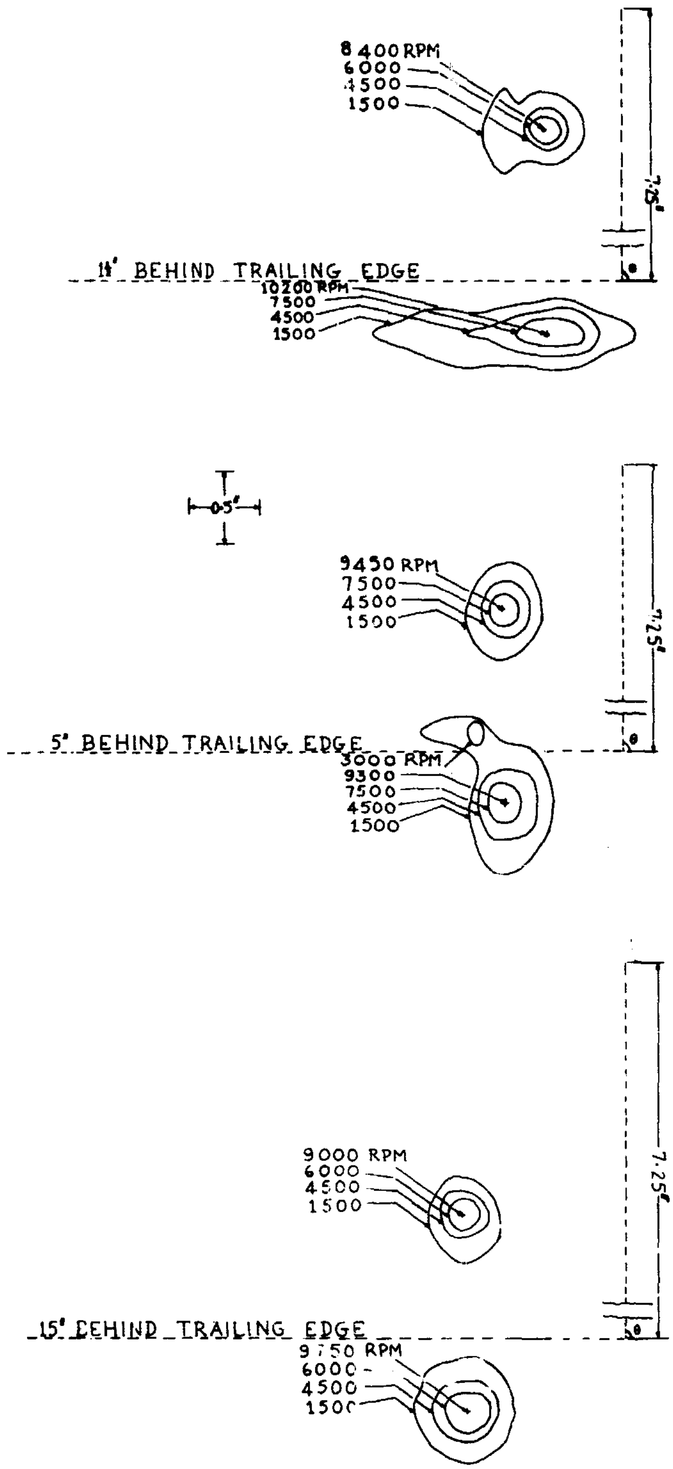

FIGURE 15 VORTICITY CONTOURS FOR DROOPED TIP WING, θ = 90°

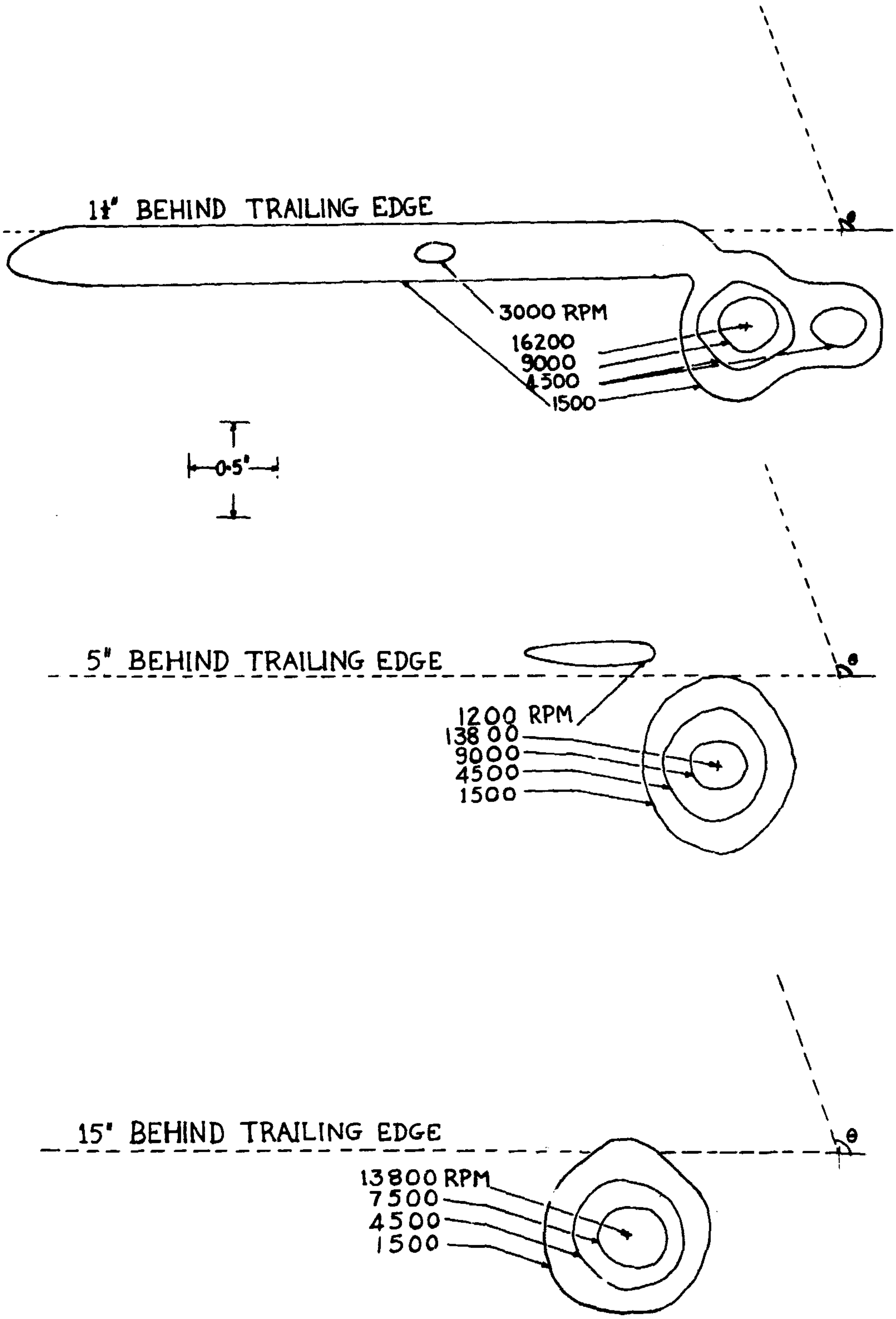

FIGURE 16 VORTICITY CONTOURS FOR DROOPED TIP WING, θ = 110°

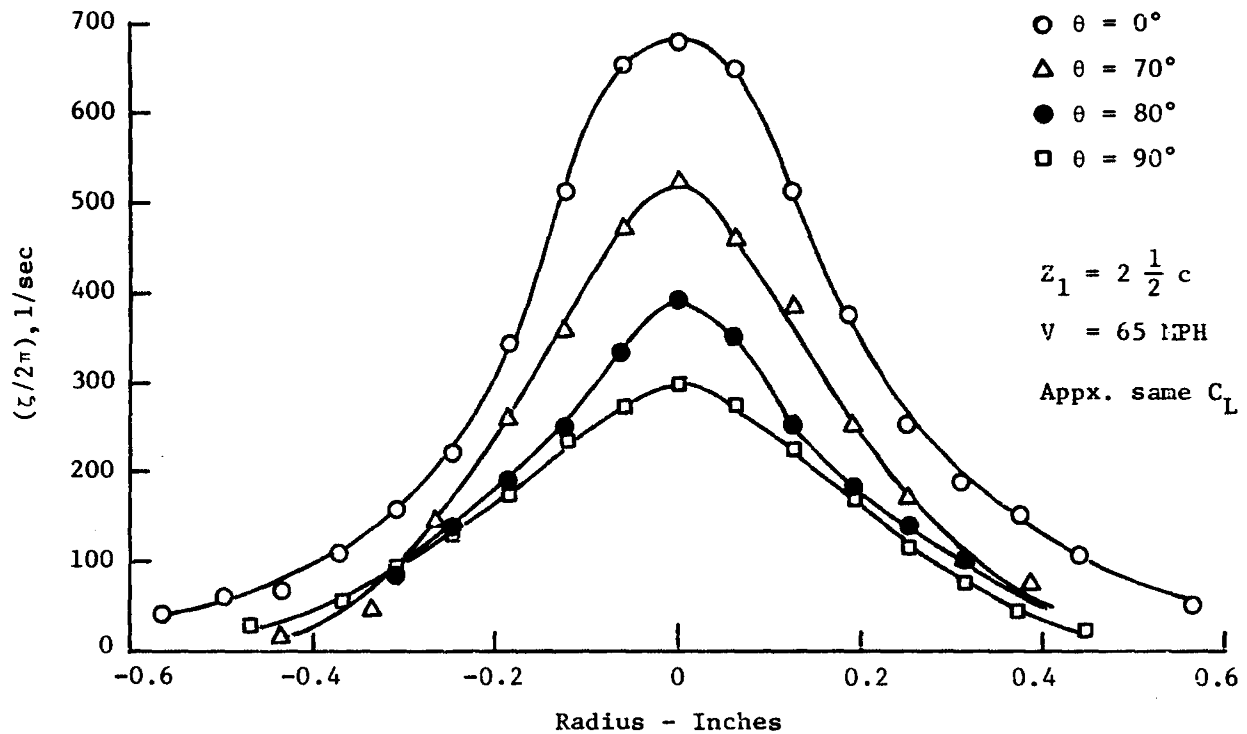

FIGURE 17 VORTICITY DISTRIBUTION THROUGH THE ROLLED-UP TIP VORTEX OF MODEL WINGS

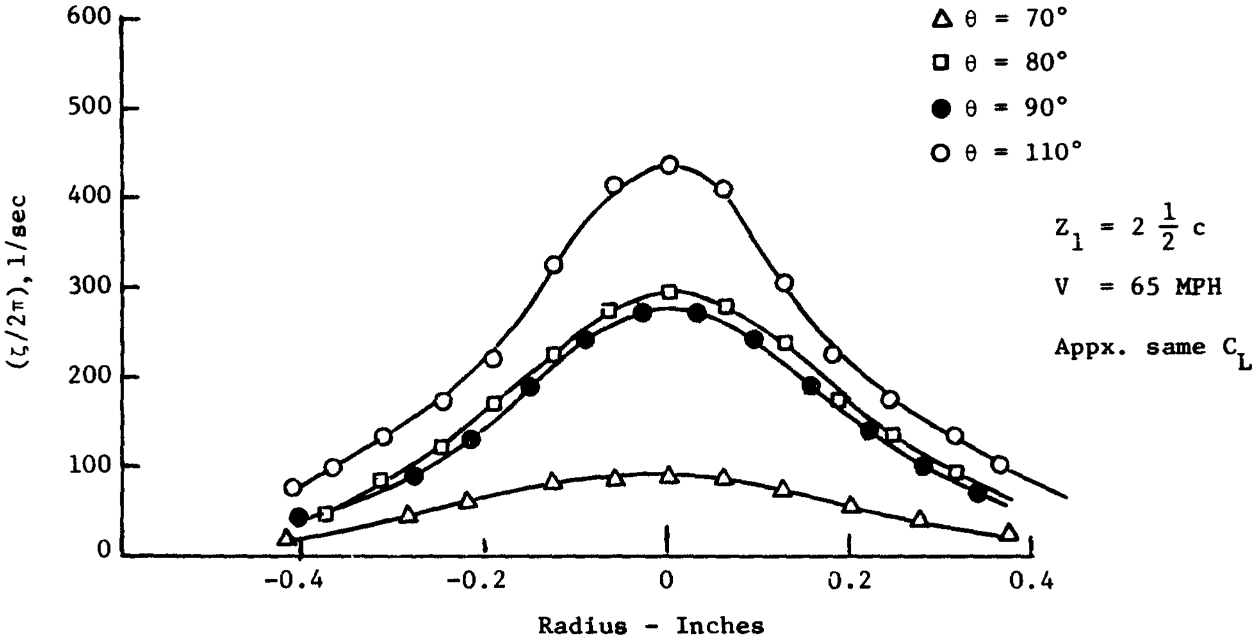

FIGURE 18 VORTICITY DISTRIBUTION THROUGH THE ROLLED-UP VORTEX AT THE HINGE LINE OF THE DROOP OF MODEL WINGS

indicates that the stronger vortex is located at the hinge line of droop. In the case of the wing with a droop angle of 90° there are two vortices, one at the tip and the other at the hinge line of the droop, though the predicted load distribution indicates only one vortex at the hinge line.

From the contours of constant vorticity it is seen that the flow is approximately axisymmetric in the rolled-up vortex. The vorticity, defined as the curl of the velocity vector, in polar coordinates is written as

$$\zeta = \frac{\partial v}{\partial r} + \frac{v}{r} - \frac{1}{r}\frac{\partial u}{\partial \theta} \tag{8}$$

where u is the velocity component in the r-direction

v is the velocity component normal to u.

For axisymmetric flow $\partial u/\partial\theta = 0$, the induced velocity v(R) at any radius R is

$$v(R) = \frac{1}{R}\int_0^R r\,\zeta\,dr \tag{9}$$

where ζ is the vorticity at any radius r, in radians/sec. In polar coordinates the Navier-Stokes equations of motion for two-dimensional axisymmetric flow can be written, in terms of vorticity as

$$\frac{\partial \zeta}{\partial t} = \nu\left[\frac{\partial^2 \zeta}{\partial r^2} + \frac{1}{r}\frac{\partial \zeta}{\partial r}\right] . \tag{10}$$

One possible solution of equation (10) is

$$\zeta = \frac{\Gamma_o}{4\pi\nu t} e^{-r^2/4\nu t} . \tag{11}$$

Substituting equation (11) into equation (9) the tangential velocity becomes

$$v(r) = \frac{\Gamma_o}{4\pi\nu t} (1 - e^{-r^2/4\nu t}) \tag{12}$$

which is known as Lamb's solution.

To fit the vorticity data obtained from the experimental investigation, an exponential similar to equation (11) was used

$$\zeta = \zeta_o e^{-(\frac{r}{w})^n \log_e 2} \tag{13}$$

where ζ_o is the maximum vorticity and

w is the "width" of the vortex, defined as the value of r for which $\zeta = \zeta_o/2$.

A computer program was written to obtain the values of w and n from the known values of ζ_o and ζ for two values of r. Using these values of w and n, ζ and v (by numerical integration) were obtained as a function of r.

For $r = \infty$ the total vortex strength Γ_∞ is given by

$$\Gamma_\infty = \int_0^\infty 2\pi r \zeta \, dr = \left[\frac{2\pi\zeta_o w^2}{n(\ln 2)^{2/n}} \right] \gamma(2/n) \tag{14}$$

where $\gamma(2/n)$ = gamma function of argument (2/n).

By the proper choice of the value of n in equation (13) the expression could be made to fit all of the experimental data. Figure 19 shows a typical fit of the exponential curve to the test data points. Table 3 gives the values of w, n and Γ_∞ for the tested model wings. In general, the values of n and w are higher for the tip vortices than for the hinge line vortices, indicating that the distribution of vorticity in the tip vortices is more "pointed." Table 4 gives values of the core radius a, (radius where v(r) is a maximum) and $\Gamma(a)$, the circulation at the radius a and the ratio $\Gamma(a)/\Gamma_\infty$. The value of $\Gamma(a)/\Gamma_\infty$ for rectangular wing is 0.572 which is of the order of the value predicted in Reference 9. As can be seen in this table, the core size of the tip vortex is, in general, larger than the core size of the vortex at the hinge line of the droop.

A calibration coefficient of 0.78 taken from Reference 11, was used in the calculation of induced velocity to take into account the frictional losses in the vorticity meter. This factor corresponds to the test velocity of 65 mph. Figures 20 and 21 show the variation of induced velocity with the vortex radius, for the wing models at the same lift, obtained by integrating the vorticity. These figures show that the induced velocity in the tip vortex decreases as the droop angle increases from 0° to 90° and the induced velocity in the hinge line vortex increases as the droop angle increases from 70° to 110°.

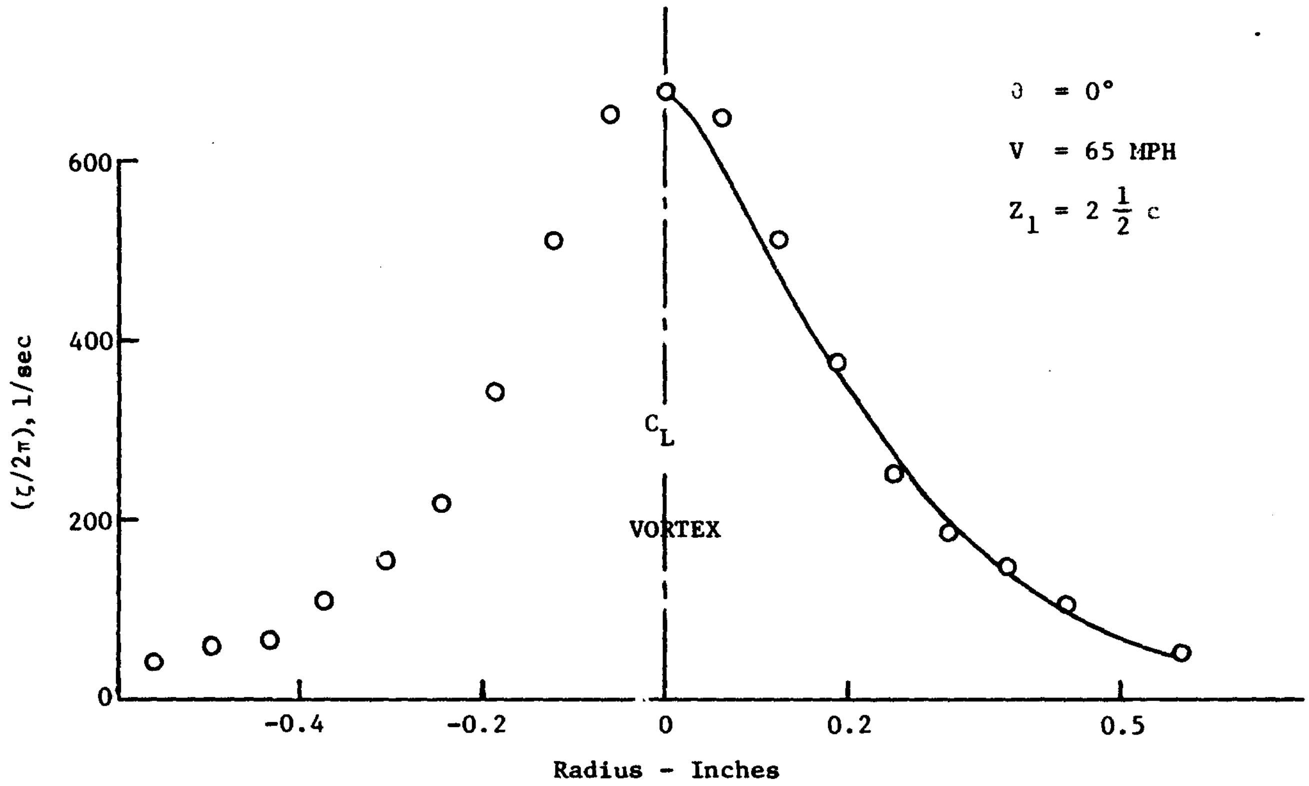

FIGURE 19 EXPONENTIAL FIT OF DATA

TABLE 3

VALUES OF VORTEX WIDTH, CIRCULATION AND "n" FOR THE TESTED WINGS

			TIP VORTEX	
θ	n	w (inches)	Γ_∞ (ft^2/sec) (from exponential fit)	Γ_{EXPTL} (ft^2/sec)
0°	1.32	0.2011	8.83	8.24
70°	1.33	0.1746	5.01	4.38
80°	1.16	0.1785	5.05	4.08
90°	1.75	0.2187	3.2	3.87

			HINGE LINE VORTEX	
θ	n	w (inches)	Γ_∞ (ft^2/sec) (from exponential fit)	Γ_{EXPTL} (ft^2/sec)
70°	2.50	0.30	1.387	1.68
80°	1.55	0.2275	3.826	3.62
90°	1.44	0.210	3.47	3.54
110°	1.24	0.1935	5.84	5.44

TABLE 4

VALUES OF CORE RADIUS AND CIRCULATION FOR THE TESTED WINGS

TIP VORTEX

θ	a (inches)	Γ(a) (ft^2/sec)	Γ_∞ (ft^2/sec) (from exponential fit)	$\Gamma(a)/\Gamma_\infty$
0°	0.3	5.05	8.83	0.572
70°	0.275	3.41	5.01	0.671
80°	0.325	3.103	5.05	0.614
90°	0.325	2.883	3.2	0.9

HINGE LINE VORTEX

θ	a (inches)	Γ(a) (ft^2/sec)	Γ_∞ (ft^2/sec) (from exponential fit)	$\Gamma(a)/\Gamma_\infty$
70°	0.375	1.47	1.387	1.055
80°	0.325	2.68	3.826	0.7
90°	0.35	2.81	3.47	0.81
110°	0.375	4.53	5.84	0.765

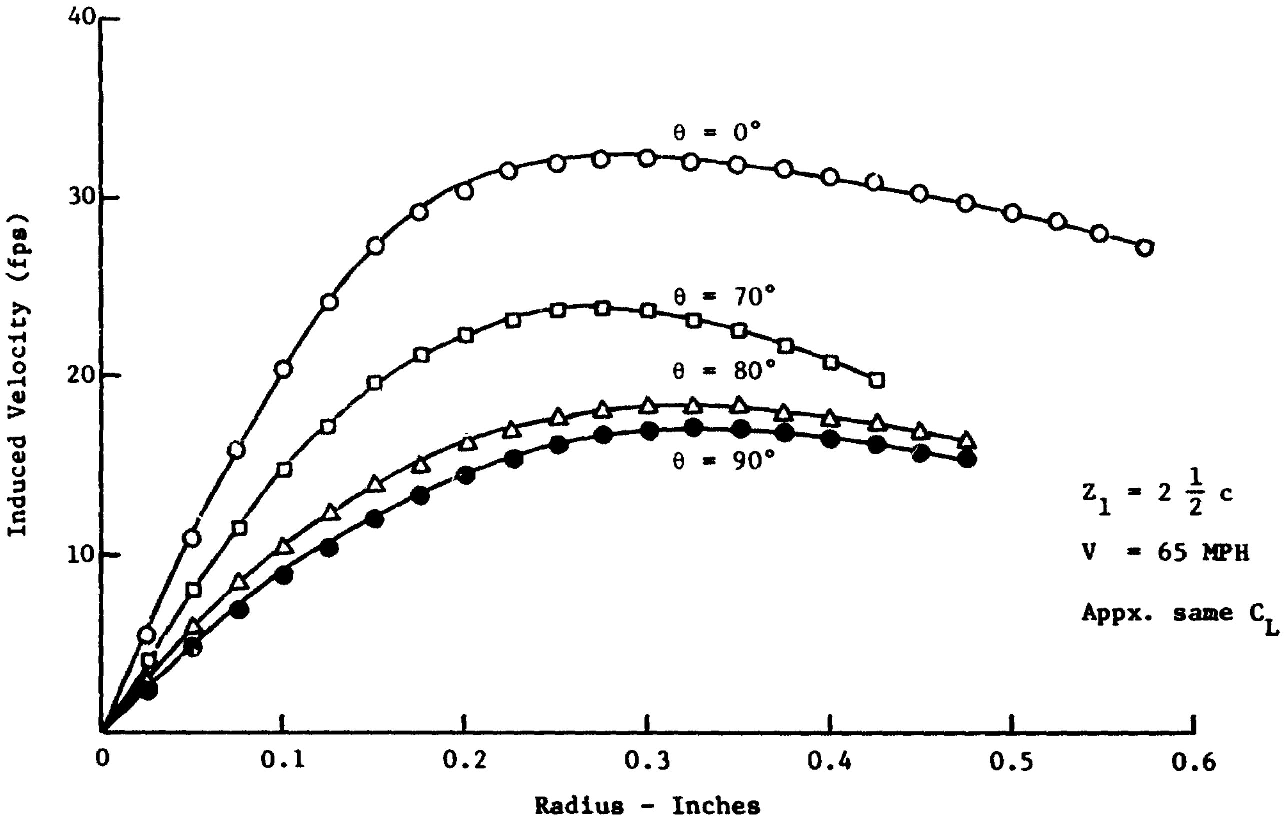

FIGURE 20 INDUCED VELOCITY IN THE ROLLED-UP TIP VORTEX OF MODEL WINGS

Figures 22 and 23 present the radial distribution of circulation through the tip and hinge line vortices of the model wings as determined from the measured vorticity distribution.

The data of these Figures 22 and 23 replotted against $\ln r$ are shown in Figures 24 and 25. As predicted by Hoffman and Joubert, Reference 28, these figures exhibit a constant slope over a large radial extent.

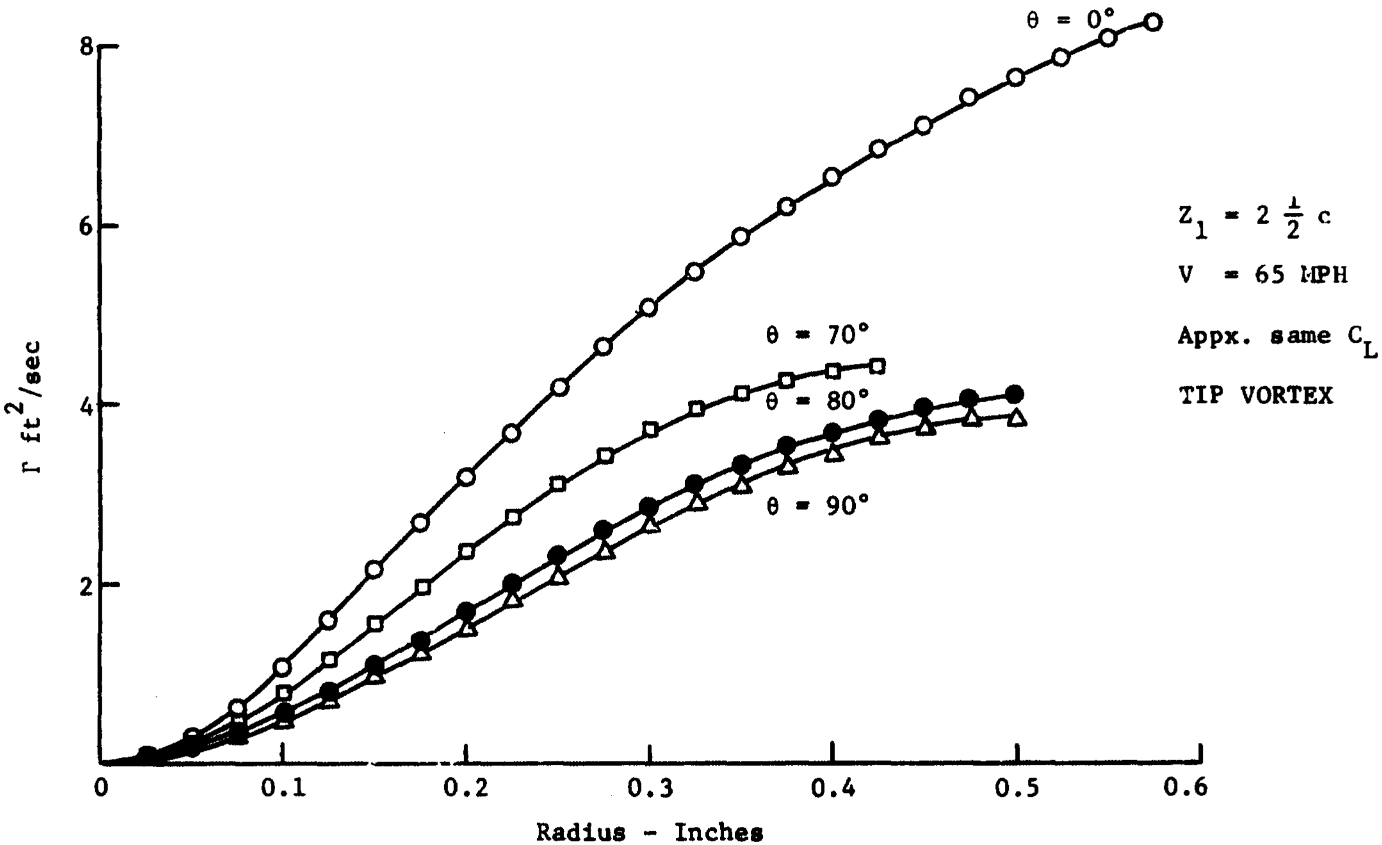

FIGURE 22 RADIAL DISTRIBUTION OF CIRCULATION THROUGH THE ROLLED-UP VORTEX

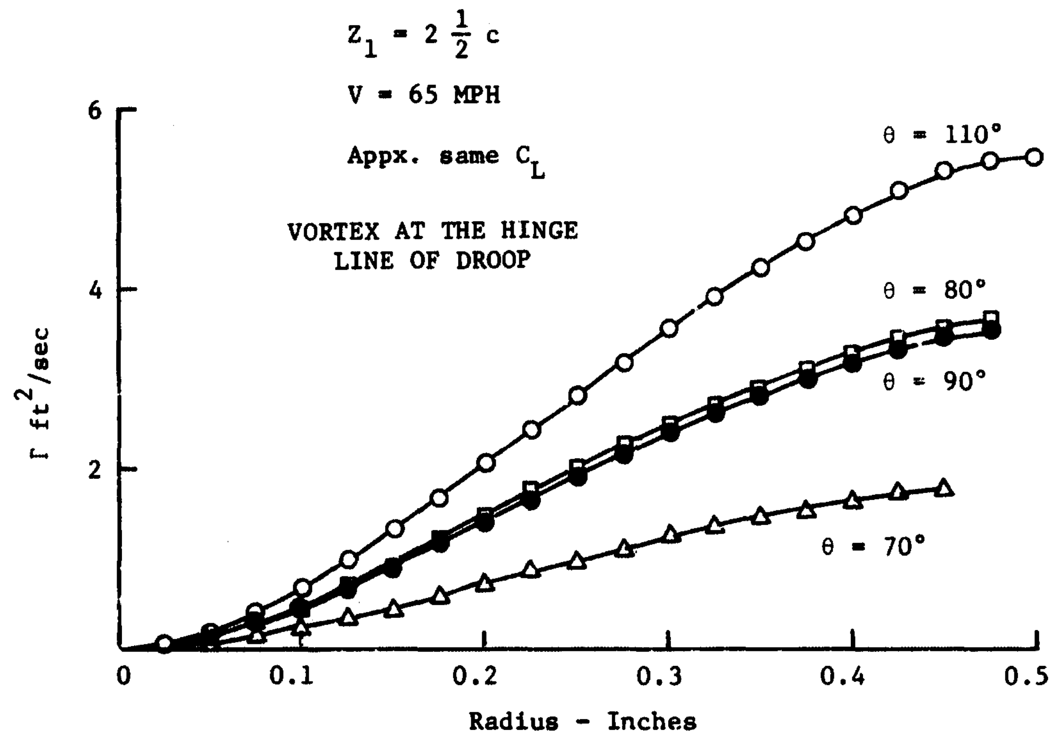

FIGURE 23 RADIAL DISTRIBUTION OF CIRCULATION THROUGH THE ROLLED-UP VORTEX

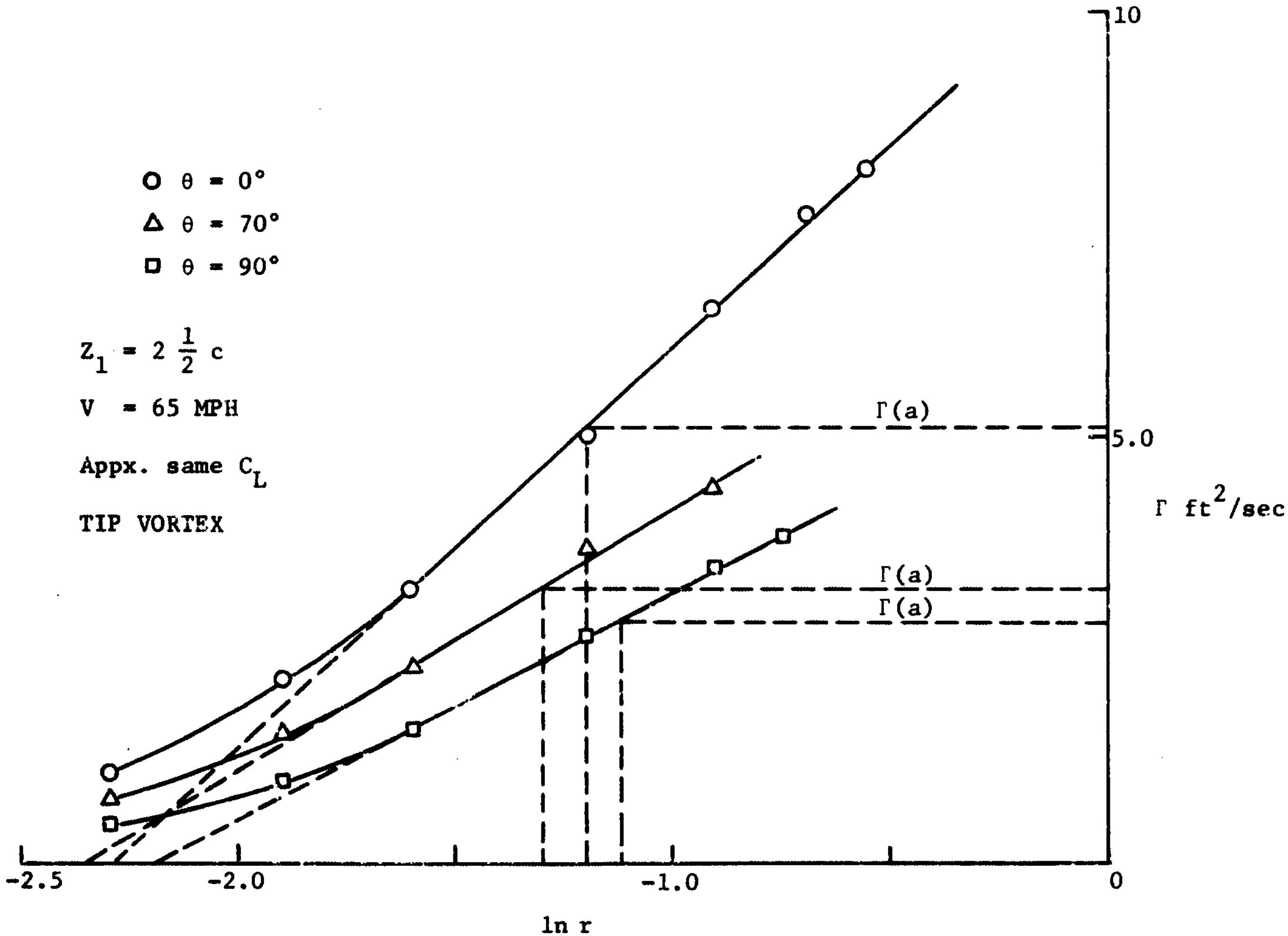

FIGURE 24 CIRCULATION VS. ln r FOR MODEL WINGS

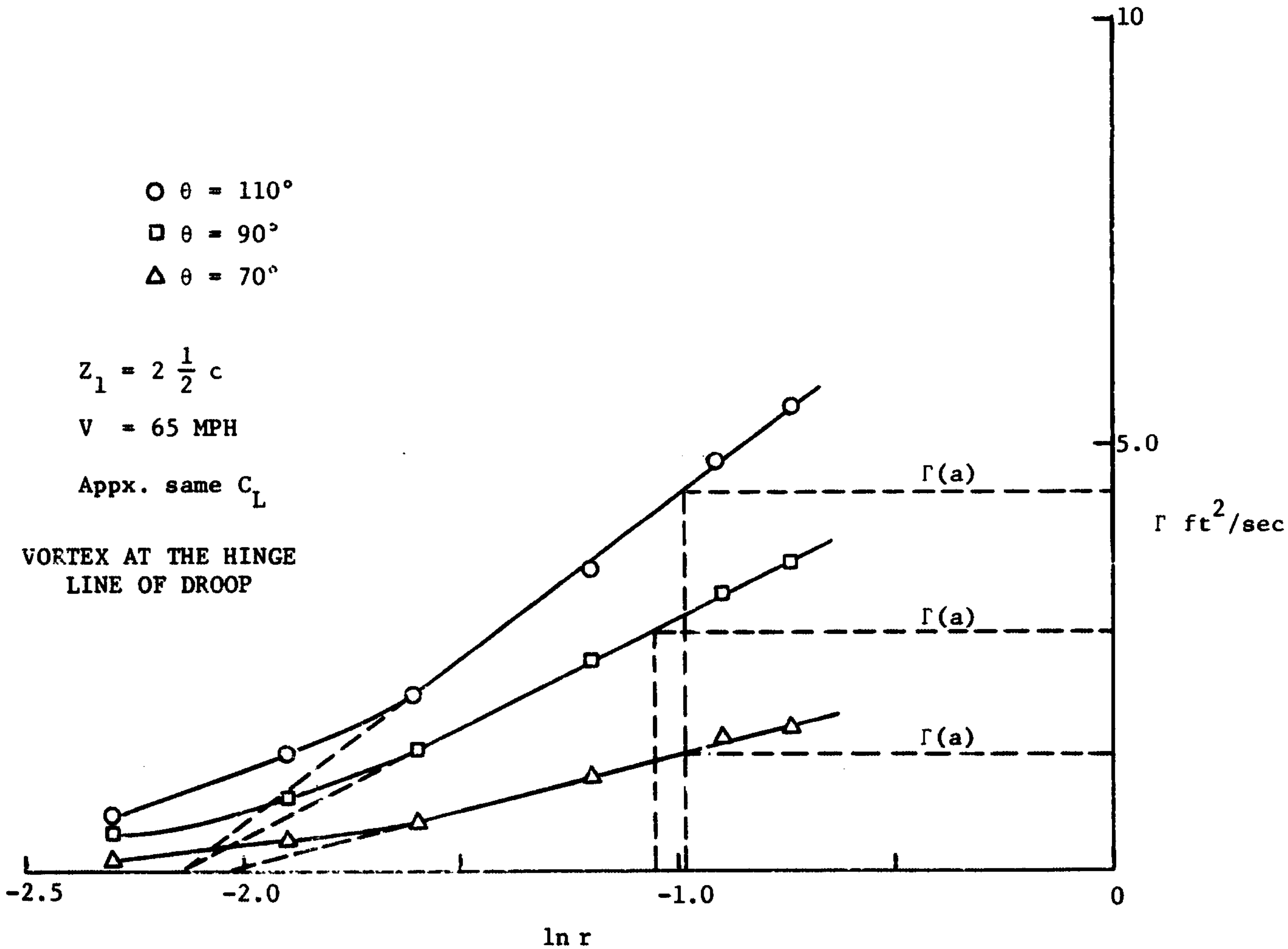

FIGURE 25 CIRCULATION VS. ln r FOR MODEL WINGS

CHAPTER VI

CONCLUSIONS

The foregoing analytical investigation presents Falkner's vortex lattice method of determining the spanwise load distribution on wings of any planform. The spanwise load distribution on wings with drooped tips was calculated by this vortex lattice theory. Experiments were made in the wind tunnel to measure the vorticity field behind the drooped tip wing models. The following conclusions can be drawn from this investigation:

(1) The spanwise load distribution, qualitatively, gives an idea of the location and the strength of the rolled-up vortex.

(2) With the increase in droop angle from 0° to 110° the maximum vorticity in the rolled-up tip vortex decreases.

(3) With the increase in droop angle from 70° to 110° the maximum vorticity in the rolled-up vortex at the hinge line of the droop increases.

(4) For droop angles of 90° and less two distinct vortices, one at the tip and the other at the hinge line of the droop, are present.

(5) The core size of the vortex at the tip is larger than the core size of the vortex at the hinge line of the droop.

(6) At droop angles greater than about 45° the lift of the drooped tip wing is considerably less than that of the plain rectangular wing, at the same angle of attack.

(7) A droop angle of approximately 90° appears to result in the minimum value of induced velocity in the vortex core.

REFERENCES

1. Falkner, V. M. "The Calculations of Aerodynamic Loading on Surfaces of Any Shape," ARC, R&M No. 1910 (1941)

2. Falkner, V. M. "The Solution of Lifting Plane Problems by Vortex Lattice Theory," ARC, R&M No. 2591 (1947)

3. Lehrian, E. D. "A Calculation of the Complete Downwash in Three Dimensions due to a Rectangular Vortex," ARC, R&M No. 2771

4. Sprieter, J. R. and Sacks, A. H. "The Rolling Up of the Trailing Vortex Sheet and its Effect on the Downwash Behind Wings," Jour. Aero. Sci., 18, 21 (1951)

5. Jenney, D. S., Olson, J. R., and Landgrebe, A. J., "A Reassessment of Rotor Hovering Performance Prediction Methods," American Helicopter Society 23rd Annual National Forum, Sikorsky Aircraft Division of United Aircraft Corporation, May 10-12, 1967

6. Lehman, A. F. "Model Studies of Helicopter Rotor Flow Problems in a Water Tunnel," American Helicopter Society 24th Annual National Forum, Water Tunnel Division, Oceanics, Inc., May 8-10, 1968

7. Leverton, J. W. Helicopter Noise-Blade Slap Part 1; Review and Theoretical Study, NASA CR-1221, October 1968

8. Schlegel, R. G. and Bausch, W. E. "Helicopter Rotor Noise Prediction and Control," American Helicopter Society 24th Annual National Forum, Sikorsky Aircraft Division of United Aircraft Corporation, May 8-10, 1968

9. McCormick, B. W., Tangler, J. M., and Sherrieb, H. E., "Structure of Trailing Vortices," Journal of Aircraft, May-June 1968

10. McCormick, B. W. "Aerodynamics of V/STOL Aircraft," Academic Press, 1967

11. Spencer, R. H., Sternfeld, H., and McCormick, B. W. "Top Vortex Core Thickening for Application to Helicopter Rotor Noise Reduction," TR 66-1, September 1966, USVAAVLABS

12. Weissinger, J. "The Lift Distribution of Swept-back Wings," NACA TM No. 1120

13. Falkner, V. M. "Calculated Loadings due to Incidence of a Number of Straight and Swept-back Wings," ARC, R&M No. 2596 (1952)

14. May, D. M. "The Development of a Vortex Meter," M.S. Thesis, The Pennsylvania State University, June 1964

15. Spivey, R. F. "Blade Tip Aerodynamics--Profile and Planform Effects," American Helicopter Society 24th Annual National Forum, Bell Helicopter Company, May 8-10, 1968

16. Jones, R. T. and Cohen, D. "High Speed Wing Theory," Princeton Aeronautical Paperbacks, Number 6, 1960

17. Simons, I. A. "Some Aspects of Blade/Vortex Interaction on Helicopters in Forward Flight," Journal of Sound and Vibration, Vol. 4, Number 3, pp. 268-281, 1966

18. Leverton, J. W. and Taylor, F. W. "Helicopter Blade Slap," Journal of Sound and Vibration, Vol. 4, Number 3, pp. 345-357, 1966

19. Davenport, F. J. "A Method for Computation of the Induced Velocity Field of a Rotor in Forward Flight, Suitable for Application to Tandem Rotor Configurations," Journal of American Helicopter Society, 9, 1964

20. Multhopp, H. "A Method for Calculating the Lift Distribution of Wings (Subsonic Lifting Surface Theory), ARC, R&M No. 2884

21. Jones, J. P. "An Extended Lifting Line Theory for the Loads on a Rotor Blade in the Vicinity of a Vortex," M.I.T. Aero Elastic and Structures Laboratory Report TR-123-3, December 1965

22. Miller, R. H. "Rotor Blade Harmonic Airloading," AIAA Journal, July 1964

23. John De Young. "Rule of Thumb Equation for Predicting Lifting Surface-Theory Values of Lift," J. Aeron. Sci., 24, 8,629 August 1957

24. Smith, H. A. and Loftin, L. K. "Aerodynamic Characteristics of 15 NACA Airfoil Sections of Seven Reynolds Numbers from 0.7×10^6 to 9×10^6," NACA TN 1945, October 1949

25. Heyson, H. H. and Critzos, C. C. "Aerodynamic characteristics of NACA 0012 Airfoil Section at Angles of Attack from 0° to 180°," NACA TN 3361, January 1955

26. Ollerhead, J. B. and Lawson, M. V. "Problems of Helicopter Noise Estimation and Reduction," Presented at the AIAA/AHS VTOL Research, Design, and Operations Meeting, February 1969

27. Cox, C. R. "Measurements in Wind Tunnels," Proceedings of the Third CAL/AVLABS Symposium, Vol. 1, June 1969

28. Hoffman, E. R. and Joubert, P. N. "Turbulent Line Vortices," Journal of Fluid Mechanics, Vol. 16, Pt. 3, July 1963, pp. 395-411

29. Lamb, H. "Hydrodynamics," 6th ed., Dover, New York, 1945, pp. 591-592